AIMS Mathematics, 11(3): 7695–7739.
DOI: 10.3934/math.2026317
Received: 20 December 2025
Revised: 23 February 2026
Accepted: 27 February 2026
Published: 24 March 2026

http://www.aimspress.com/journal/Math

Research article

Ecological and epidemiological thresholds in a predator–prey system with cross-infection: stability, bifurcations, and reaction-diffusion dynamics

Faisal Muteb K. Almalki[1], Ghaliah Alhamzi[2], Mona Bin-Asfour[2], Emad Solouma[2,*], Najat Almutairi[3], Ali Sarrah[1] and Sayed Saber[1,4]

[1] Department of Mathematics, Faculty of Science, Al-Baha University, Al-Baha 65779, Saudi Arabia

[2] Department of Mathematics and Statistics, College of Science, Imam Mohammad Ibn Saud Islamic University (IMSIU), Riyadh 11623, Saudi Arabia

[3] Department of Mathematics, College of Science, Qassim University, Buraidah, Saudi Arabia

[4] Department of Mathematics and Computer Science, Faculty of Science, Beni-Suef University, Egypt

* **Correspondence:** Email: gyalhamzi@imamu.edu.sa.

Abstract: This paper investigates a four–dimensional predator–prey model with cross–species infection and Holling type II functional response. The model incorporates logistic growth for susceptible prey, susceptible–infected (SI)–type disease transmission with mass–action incidence, and a biologically realistic mechanism by which predators become infected through consumption of infected prey. We derive five key ecological and epidemiological threshold parameters governing predator persistence and disease invasion in different ecological scenarios. Analytical results establish positivity, boundedness, and conditions for the existence, feasibility, and stability of all equilibria. These include disease–free coexistence, endemic prey–only, and full endemic coexistence states. Global stability of the disease–free coexistence equilibrium is obtained using the Lyapunov method. Bifurcation analyses reveal transcritical, Hopf, and saddle–node bifurcations, explaining the transitions between extinction, stable coexistence, oscillatory dynamics, and bistability. Co–dimension–two analysis identifies organizing centers that structure the parameter space and clarifies mechanisms underlying regime shifts. Numerical simulations using MATLAB and MatCont confirm theoretical findings and illustrate diverse dynamical behaviors. These behaviors include predator extinction driven by highly infectious diseases, predation–mediated disease control, sustained oscillations, and multiplicity. Spatial extension via a reaction–diffusion framework demonstrates diffusion–driven Turing instability and pattern formation. The results provide integrated ecological and epidemiological insights into cross–infection dynamics and predator–prey coexistence.

Keywords: predator–prey interactions; cross-infection; Holling type II functional response;

bifurcation analysis; Turing patterns; spatial dynamics
Mathematics Subject Classification: 34C23, 35B36, 37G15, 92D25, 92D30

1. Introduction

Predator–prey interactions are fundamental drivers of ecological dynamics, and their complexity is profoundly amplified by infectious diseases. Pathogens can regulate population size, alter interaction strengths, induce trophic cascades, and even facilitate coexistence in otherwise unstable communities [1]. A well–documented ecological phenomenon is that predators often preferentially consume infected prey, which are typically more vulnerable due to parasite–induced behavioral, physiological, or morphological impairment [2]. Such selective predation establishes a bidirectional feedback between epidemiological processes and trophic interactions, generating rich and sometimes counter–intuitive dynamical outcomes. Understanding these coupled mechanisms is essential for predicting biodiversity persistence, outbreak regulation, and ecosystem resilience.

Mathematical modeling has been central to uncovering eco–epidemiological mechanisms. Classical predator–prey models incorporating nonlinear functional responses were initiated in [2] and later expanded through structured population theory and stability analysis [3, 4]. The introduction of infectious disease into predator–prey systems revealed significant ecological effects; in particular, [5] demonstrated that prey infection can facilitate predator persistence and stabilize coexistence.

Subsequent studies examined nonlinear transmission, ratio–dependent predation, fear effects, harvesting strategies, refuge mechanisms, and Allee dynamics [6–8]. Additional work has explored various functional responses and bifurcation structures [9–11]. The dynamics of predator–prey systems with different functional responses have been extensively analyzed [12–14]. Further investigations have considered Allee effects and Holling–type functional responses [15–17]. Stability and boundedness results have been established for modified Leslie–Gower models [18,19]. Bifurcation analysis of predator–prey systems has been advanced through various approaches [20–22]. Global dynamics of Leslie–type models have been studied [23–25]. The dynamics of predator–prey systems have been explored from multiple perspectives [26,27]. Recent work has examined bifurcations driven by generalist and specialist predation [28, 29].

More recently, spatial extensions and bifurcation–based analyses have uncovered diffusion–driven instability, pattern formation, multistability, and complex oscillatory behavior [9, 30, 31]. Seasonal forcing has been shown to induce complex dynamics such as multiple attractors and chaos [32–34]. Further studies on periodic perturbations have revealed strange attractors and bifurcation structures [35, 36]. Fractional-order modeling has been successfully employed to analyze chaos control and stability in biological systems, particularly glucose–insulin regulatory models [37–39]. Recent advances have extended these approaches to other chaotic systems, including the Newton-Leipnik system [40], the Lorenz model [41], and systems analyzed using Caputo-Fabrizio operators [42], demonstrating the effectiveness of fractal-fractional derivatives in capturing complex dynamical behaviors.

Discrete predator–prey models have attracted considerable attention due to their rich dynamical behaviors, including bifurcation, chaos, and stability switching. Several recent studies have investigated the complex dynamics of discretized predator–prey systems with various functional

responses and Allee effects [43–45]. Additional research has examined bifurcation analysis and chaos control in discrete predator–prey systems [46, 47]. Further fractional–order approaches have provided insights into stability and chaotic behavior [48–50].

Despite these advances, cross–species transmission driven explicitly by predation events remains underexplored. In particular, few models rigorously investigate the scenario where infection spills over from prey to predator during predation, while horizontal transmission among predators is absent. This small–step spillover mechanism is biologically realistic and highly relevant to early–stage zoonotic emergence, where pathogens first expand their host range through trophic interactions before adapting to efficient within–species spread. Existing eco–epidemiological models typically assume predator–to–predator transmission or treat predator infection as a secondary effect without constructing a systematic threshold framework linking ecological invasion and epidemiological reproductive processes. Consequently, the hierarchical interaction between trophic persistence and disease invasion remains insufficiently characterised.

In this work, we develop and analyze a four–dimensional predator–prey system incorporating: (i) logistic growth of susceptible prey, (ii) susceptible–infected (SI)–type mass–action transmission within prey, (iii) Holling type II predation on both susceptible and infected prey, and (iv) predator infection proportional to predation on infected prey, without horizontal spread among predators. This formulation enables the explicit investigation of spillover dynamics mediated exclusively by trophic interaction.

The main contributions to this study are as follows: First, we construct a unified hierarchical threshold framework consisting of five invasion parameters governing predator persistence and disease spread in different ecological contexts. This framework clarifies how ecological and epidemiological thresholds interact and compete. Second, we establish feasibility and local and global stability conditions for all biologically relevant equilibria using Lyapunov methods and asymptotically autonomous system theory. Third, we perform comprehensive bifurcation analyses, including codimension–one (transcritical, Hopf, and saddle–node) and codimension–two (Bogdanov–Takens and cusp) structures, which reveal the organizing mechanisms underlying transitions between stability, oscillation, and bistability. Fourth, we extend the model to a spatial reaction–diffusion system and demonstrate how Turing instability can generate spatial patterns such as spots and stripes, thereby linking infection dynamics with spatial heterogeneity.

By integrating spillover transmission mechanisms, hierarchical invasion thresholds, global stability analysis, bifurcation theory, and spatial pattern formation within a single framework, this study advances the mathematical theory of coupled ecological–epidemiological systems and provides new insights into predator–mediated pathogen emergence.

The complexity of the proposed system arises naturally from its dimension and non–linear interaction mechanisms. The four–dimensional structure, combining trophic interaction and cross–infection, introduces multiple feedback loops linking ecological growth, epidemiological transmission, and predator persistence. In particular, the coexistence equilibrium involves a Jacobian matrix whose characteristic polynomial is quartic. This permits multiple eigenvalue configurations, including pairs of purely imaginary roots and zero eigenvalues. This structural property enables codimension–one bifurcations (e.g., transcritical and Hopf) as well as higher–order degeneracy such as Bogdanov–Takens bifurcations, where both a zero eigenvalue and additional nonlinear terms organize system dynamics.

Moreover, the nonlinear Holling type II functional responses and infection terms generate non–monotonic per–capita growth rates and multiple threshold interactions. The presence of five interdependent invasion parameters creates competing persistence conditions across trophic and epidemiological processes. Such hierarchical threshold interactions produce bistability, oscillations, and chaotic dynamics, which are analytically characterized in later sections.

When spatial diffusion is incorporated, the dimensionality of the associated linearized operator further increases. Diffusion–driven instability becomes possible when the homogeneous steady state satisfies the standard Turing conditions. Hence, the model's complexity is not imposed artificially but emerges intrinsically from biologically realistic mechanisms: nonlinear predation, cross–species transmission, and coupled invasion thresholds.

The remainder of the paper is organized as follows. Section 2 presents the model formulation and assumptions. Section 3 analyzes the disease–free subsystem. Section 4 derives threshold conditions for the full model. Sections 5–9 develop the stability and bifurcation analysis. Section 10 introduces the spatial extension and pattern formation results. Section 11 discusses biological implications, and Section 12 concludes.

2. The model

We model the interaction between a prey population and a predator population, where a disease can infect both species. The total prey population is subdivided into susceptible (S) and infected (I) classes. The predator population is subdivided into susceptible (P_1) and infected (P_2) classes. The model is based on the following core assumptions:

(A1) The susceptible prey (S) exhibits logistic growth with an intrinsic rate r and carrying capacity K. Infected prey (I) do not reproduce but contribute to density–dependent regulation.
(A2) The disease in the prey is of SI–type, with transmission governed by mass–action incidence $\lambda_1 S I$. Infected individuals do not recover.
(A3) Predation follows a Holling type II functional response. The capture rates for susceptible and infected prey are α_1 and α_2, respectively, with half–saturation constants a_1 and a_2.
(A4) Susceptible predators (P_1) grow by consuming susceptible prey, with a conversion efficiency β.
(A5) Susceptible predators become infected (P_2) upon consuming infected prey. The force of infection for predators is proportional to the predation rate on infected prey, given by $\lambda_2 \left(\frac{I}{1 + a_2 I} \right)$.
(A6) Infected predators do not reproduce and suffer an increased mortality rate $\gamma_2 \geq \gamma_1$, where γ_1 is the mortality rate of susceptible predators. There is no recovery or immunity.
(A7) Infected prey are more vulnerable to predation ($\alpha_2 \geq \alpha_1$).

Under these assumptions, the dynamics are governed by the following system of ordinary differential equations (ODEs):

$$\begin{cases} S' = rS\left(1-\dfrac{S+I}{K}\right)-\lambda_1 IS-\dfrac{\alpha_1 S}{1+a_1 S}(P_1+P_2), \\ I' = \lambda_1 IS-\dfrac{\alpha_2 I}{1+a_2 I}(P_1+P_2)-\mu I, \\ P_1' = \dfrac{\beta S}{1+a_1 S}P_1-\gamma_1 P_1-\dfrac{\lambda_2 I}{1+a_2 I}P_1, \\ P_2' = \dfrac{\lambda_2 I}{1+a_2 I}P_1-\gamma_2 P_2, \end{cases} \tag{2.1}$$

where all derivatives are with respect to time t. A schematic diagram of the model transitions is given in Figure 1. All parameters are positive, and the biologically motivated inequalities $\alpha_2 \geq \alpha_1$ and $\gamma_2 \geq \gamma_1$ hold.

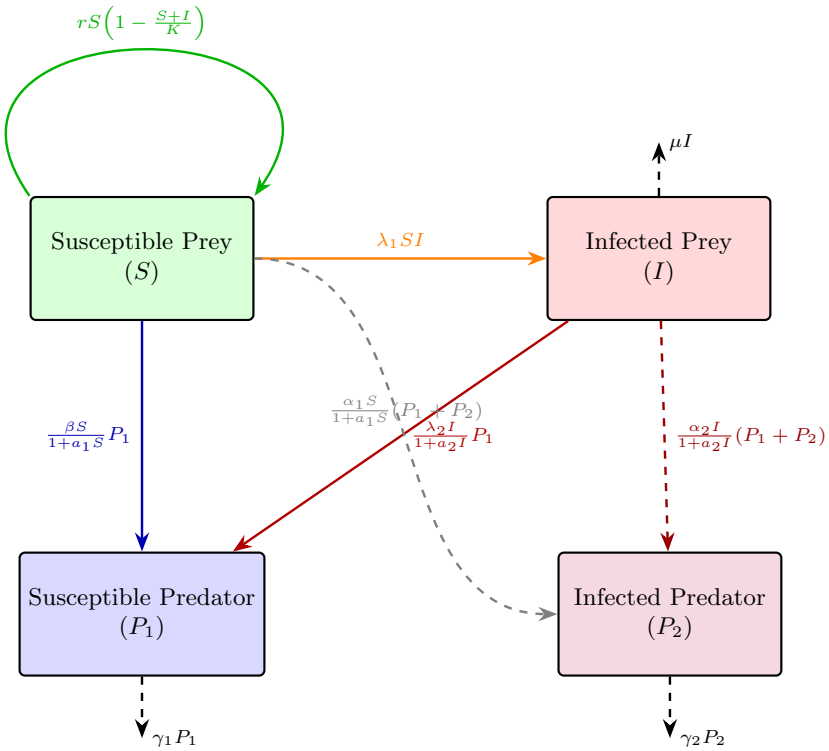

Figure 1. Schematic diagram of the predator–prey model with cross–infection. The diagram illustrates the flow of populations between compartments: susceptible prey (S), infected prey (I), susceptible predators (P_1), and infected predators (P_2). Solid arrows represent demographic processes (birth, death, and predation), while dashed arrows indicate disease transmission pathways. The model incorporates logistic growth for prey, Holling type II functional responses, and cross–species transmission during predation events.

3. The model with disease

We now analyze the full four–dimensional system (2.1). The system can exhibit up to five equilibria, categorized as trivial, boundary, and interior. The Jacobian matrix for system (2.1) is given by:

$$J(S,I,P_1,P_2)=\begin{bmatrix} J_{11} & -\left(\frac{r}{K}+\lambda_1\right)S & -\frac{\alpha_1 S}{1+a_1S} & -\frac{\alpha_1 S}{1+a_1S} \\ \lambda_1 I & J_{22} & -\frac{\alpha_2 I}{1+a_2I} & -\frac{\alpha_2 I}{1+a_2I} \\ \frac{\beta P_1}{(1+a_1S)^2} & -\frac{\lambda_2 P_1}{(1+a_2I)^2} & J_{33} & 0 \\ 0 & \frac{\lambda_2 P_1}{(1+a_2I)^2} & \frac{\lambda_2 I}{1+a_2I} & -\gamma_2 \end{bmatrix}, \tag{3.1}$$

where

$$J_{11}=r\left(1-\frac{2S+I}{K}\right)-\lambda_1 I-\frac{\alpha_1(P_1+P_2)}{(1+a_1S)^2},$$

$$J_{22}=\lambda_1 S-\frac{\alpha_2(P_1+P_2)}{(1+a_2I)^2}-\mu,$$

$$J_{33}=\frac{\beta S}{1+a_1S}-\gamma_1-\frac{\lambda_2 I}{1+a_2I}.$$

3.1. Trivial and boundary equilibria

(1) **Trivial equilibrium: $\mathbf{E_0}=(0,0,0,0)$**
This equilibrium always exists but is unstable.

(2) **Prey–only rquilibrium: $\mathbf{E_B}=(K,0,0,0)$**
The basic reproduction number for disease in prey is:

$$R_0=\frac{K\lambda_1}{\mu}. \tag{3.2}$$

Lemma 3.1. *(i) If $R_0<1$ and $R_1<1$, then $\mathbf{E_B}$ is locally asymptotically stable.*
(ii) If $R_0>1$ or $R_1>1$, then $\mathbf{E_B}$ is unstable.

(3) **Endemic prey–only equilibrium: $\overline{\mathbf{E}}_\mathbf{B}=(\overline{S},\overline{I},0,0)$**
The predator invasion number at the endemic state is:

$$\overline{R}_1=\frac{\beta\overline{S}}{\gamma_1(1+a_1\overline{S})}. \tag{3.3}$$

Lemma 3.2. *(i) If $\overline{R}_1<1+\dfrac{\lambda_2\overline{I}}{\gamma_1(1+a_2\overline{I})}$, then $\overline{\mathbf{E}}_\mathbf{B}$ is locally asymptotically stable.*

(ii) If $\overline{R}_1>1+\dfrac{\lambda_2\overline{I}}{\gamma_1(1+a_2\overline{I})}$, then $\overline{\mathbf{E}}_\mathbf{B}$ is unstable.

(4) **Disease–free coexistence:** $\mathbf{E}^*_{\mathbf{B}} = (S^*, 0, P_1^*, 0)$
The disease invasion number at the coexistence state is:

$$R_0^* = \frac{\lambda_1 S^*}{\alpha_2 P_1^* + \mu}. \tag{3.4}$$

Lemma 3.3. *(i) If* $R_0^* < 1$ *and* $1 < R_1 < 1 + \dfrac{\beta}{a_1\gamma_1(1+a_1K)}$, *then* $\mathbf{E}^*_{\mathbf{B}}$ *is locally asymptotically stable.*
(ii) If $R_0^* > 1$ *or* $R_1 > 1 + \dfrac{\beta}{a_1\gamma_1(1+a_1K)}$, *then* $\mathbf{E}^*_{\mathbf{B}}$ *is unstable.*

3.2. Interior equilibrium

The positive interior equilibrium $\widetilde{\mathbf{E}} = (\widetilde{S}, \widetilde{I}, \widetilde{P}_1, \widetilde{P}_2)$ represents endemic coexistence of all populations.

Lemma 3.4. *Let* $\widetilde{R}_1 = \dfrac{\beta\widetilde{S}}{\gamma_1(1+a_1\widetilde{S})}$. *If* $\widetilde{S}$ *satisfies* $\overline{S} < \widetilde{S}$ *and* $\widetilde{S} + \widetilde{I} < K$, *and if* $1 < \widetilde{R}_1 < 1 + \dfrac{\lambda_2}{a_2\gamma_1}$, *then* $\widetilde{\mathbf{E}}$ *exists and is given by*

$$\widetilde{I} = \frac{\widetilde{S}(\beta - a_1\gamma_1) - \gamma_1}{\lambda_2(1+a_1\widetilde{S}) - a_2[\widetilde{S}(\beta - a_1\gamma_1) - \gamma_1]},$$

$$\widetilde{P}_1 = \frac{1}{\alpha_2}(\lambda_1\widetilde{S} - \mu)(1+a_2\widetilde{I})\left[1 + \frac{\lambda_2}{\gamma_2}\left(\frac{\widetilde{I}}{1+a_2\widetilde{I}}\right)\right]^{-1},$$

$$\widetilde{P}_2 = \frac{\lambda_2}{\gamma_2}\left(\frac{\widetilde{I}}{1+a_2\widetilde{I}}\right)\widetilde{P}_1.$$

When $(\beta - a_1\gamma_1) - \lambda_2 = 0$, the equilibrium is unique. Otherwise, uniqueness depends on the sign of $b^2 - 4ac$. Stability will be explored numerically in Section 6.

4. Ecological and disease threshold parameters

The biological significance of the five threshold parameters is discussed below.

4.1. Biological interpretation

(1) **Predator invasion number** (R_1):

$$R_1 = \frac{\beta K}{\gamma_1(1+a_1K)}. \tag{4.1}$$

This determines predator persistence in the disease–free system, representing the average number of newborn predators per predator.

(2) **Disease basic reproduction number** (R_0):

$$R_0 = \frac{K\lambda_1}{\mu}. \tag{4.2}$$

This governs disease establishment in prey, where $K\lambda_1$ is the infection rate and $1/\mu$ is the infectious period.

(3) **Endemic predator invasion number ($\overline{R}_1$)**:

$$\overline{R}_1 = \frac{\beta \overline{S}}{\gamma_1(1 + a_1\overline{S})}. \tag{4.3}$$

This represents the ecological reproduction number for predators when disease is endemic in prey.

(4) **Coexistence disease reproduction number (R_0^*)**:

$$R_0^* = \frac{\lambda_1 S^*}{\alpha_2 P_1^* + \mu}. \tag{4.4}$$

This measures disease invasion potential when infected prey enter a disease–free coexistence environment.

(5) **Endemic coexistence number ($\widetilde{R}_1$)**:

$$\widetilde{R}_1 = \frac{\beta \widetilde{S}}{\gamma_1(1 + a_1\widetilde{S})}. \tag{4.5}$$

This governs predator persistence under endemic coexistence conditions.

4.2. Relationships and ecological implications

Define $R_1(S) = \dfrac{\beta S}{\gamma_1(1 + a_1 S)}$. Then:

$$R_1 = R_1(K), \quad \overline{R}_1 = R_1(\overline{S}), \quad \widetilde{R}_1 = R_1(\widetilde{S}). \tag{4.6}$$

The hierarchical relationship $\overline{R}_1 < \widetilde{R}_1 < R_1$ indicates that disease presence makes predator persistence increasingly difficult. When $R_0^* < 1$ but $R_0 > 1$, populations may persist with disease fluctuating in a limit cycle without endemic establishment. This demonstrates that $R_1 > 1$ alone no longer guarantees predator–prey coexistence in the presence of disease. The phenomenon of dual threshold parameters has been observed in similar systems [5].

5. Existence, feasibility, and stability of equilibria

5.1. Preliminaries: invariance and boundedness

Lemma 5.1 (Positivity and boundedness)**.** *For nonnegative initial conditions* $(S(0), I(0), P_1(0), P_2(0)) \in \mathbb{R}^4_+$*, all trajectories of model* (2.1) *remain nonnegative and uniformly bounded in* $\mathbb{R}^4_+$.

Proof. Positivity follows from examining the vector field on each boundary plane. For boundedness, consider the total prey population $N = S + I$:

$$N' = rS\left(1-\frac{N}{K}\right)-\mu I-\frac{\alpha_1 S}{1+a_1 S}(P_1+P_2)-\frac{\alpha_2 I}{1+a_2 I}(P_1+P_2)$$
$$\leq rN\left(1-\frac{N}{K}\right)-\mu_{\min} N,$$

where $\mu_{\min} = \min(0,\mu)$. By comparison, $\limsup_{t\to\infty} N(t) \leq M_N$. Similarly, the total predator population $P = P_1 + P_2$ satisfies:

$$P' \leq \frac{\beta}{a_1} P_1 - \gamma_{\min} P,$$

where $\gamma_{\min} = \min(\gamma_1, \gamma_2)$, ensuring boundedness. □

5.2. Equilibria and their stability

5.2.1. Boundary equilibria

Theorem 5.2 (Stability of boundary equilibria)**.** *The system* (2.1) *has the following boundary equilibria:*

(1) $\mathbf{E}_0 = (0,0,0,0)$ *is always unstable (a saddle).*
(2) $\mathbf{E}_B = (K,0,0,0)$ *is locally asymptotically stable if and only if:*

$$R_0 < 1 \quad \textit{and} \quad R_1 < 1.$$

5.2.2. Disease–free coexistence equilibrium

Theorem 5.3 (Disease–free coexistence)**.** *The equilibrium* $\mathbf{E}_B^* = (S^*, 0, P_1^*, 0)$*, where*

$$S^* = \frac{\gamma_1}{\beta - a_1\gamma_1} \quad \textit{and} \quad P_1^* = \frac{r}{\alpha_1}\left(1-\frac{S^*}{K}\right)(1+a_1 S^*),$$

exists if and only if $R_1 > 1$*. It is locally asymptotically stable if*

$$1 < R_1 < 1 + \frac{\beta}{a_1\gamma_1(1+a_1 K)} \quad \textit{and} \quad R_0^* < 1.$$

Proof. Existence follows from $S^* > 0$ and $P_1^* > 0$. The Jacobian at $\mathbf{E}_B^*$ has block structure where the eigenvalue $A_{22} = (\alpha_2 P_1^* + \mu)(R_0^* - 1)$ determines disease invasion stability. The (S, P_1) subsystem stability is governed by R_1. □

5.2.3. Endemic and interior equilibria

Theorem 5.4 (Endemic states)**.** *The system admits:*

(1) $\overline{\mathbf{E}}_B = (\overline{S}, \overline{I}, 0, 0)$*, which exists if* $R_0 > 1$ *and is locally asymptotically stable if* $\overline{R}_1 < 1 + \frac{\lambda_2 \overline{I}}{\gamma_1(1+a_2\overline{I})}$*;*
(2) $\widetilde{\mathbf{E}} = (\widetilde{S}, \widetilde{I}, \widetilde{P}_1, \widetilde{P}_2)$*, which exists under Lemma 3.4 conditions. Stability is determined numerically.*

5.3. Global stability of disease–free coexistence

Theorem 5.5 (Global stability of $\mathbf{E}_{\mathrm{B}}^*$)**.** *Assume:*

(1) The disease–free subsystem has a globally asymptotically stable equilibrium $E^* = (S^*, P_1^*)$;
(2) $R_0^* < 1$.

Then $\mathbf{E}_{\mathrm{B}}^*$ is globally asymptotically stable in $\mathbb{R}_+^4$.

Proof. Consider the Lyapunov function candidate:

$$V(S, I, P_1, P_2) = \left(\int_{S^*}^{S} \frac{\xi - S^*}{\xi}\, d\xi + \int_{P_1^*}^{P_1} \frac{\eta - P_1^*}{\eta}\, d\eta \right) + k_1 I + k_2 P_2,$$

with $k_1, k_2 > 0$. The derivative satisfies:

$$\dot{V} \leq \dot{V}_1 + k_1(\lambda_1 S I - \mu I) + k_2 \left(\frac{\lambda_2 I}{1 + a_2 I} P_1 - \gamma_2 P_2 \right).$$

As $t \to \infty$, $S(t) \to S^*$ and $P_1(t) \to P_1^*$. The limiting infected subsystem is:

$$I' \approx (\alpha_2 P_1^* + \mu)(R_0^* - 1) I,$$
$$P_2' \approx \frac{\lambda_2 I}{1 + a_2 I} P_1^* - \gamma_2 P_2.$$

Since $R_0^* < 1$, $I(t) \to 0$ and consequently, $P_2(t) \to 0$. By asymptotically autonomous systems theory, all trajectories converge to $\mathbf{E}_{\mathrm{B}}^*$. □

Theoretical stability analysis of the interior equilibrium

While the existence conditions for the interior equilibrium $\widetilde{\mathbf{E}} = (\widetilde{S}, \widetilde{I}, \widetilde{P}_1, \widetilde{P}_2)$ were established in Lemma 3.4, a complete analytical characterization of its stability requires careful theoretical treatment due to the four–dimensional nature of the system. We now provide a comprehensive theoretical stability analysis before presenting numerical verification.

Theorem 5.6 (Theoretical stability of interior equilibrium)**.** *Let $\widetilde{\mathbf{E}} = (\widetilde{S}, \widetilde{I}, \widetilde{P}_1, \widetilde{P}_2)$ be the interior equilibrium whose existence is guaranteed by Lemma 3.4. The local stability of $\widetilde{\mathbf{E}}$ is governed by the Jacobian matrix $J(\widetilde{\mathbf{E}})$ given in (3.1). The characteristic polynomial is*

$$P(\lambda) = \lambda^4 + \sigma_1 \lambda^3 + \sigma_2 \lambda^2 + \sigma_3 \lambda + \sigma_4 = 0, \tag{5.1}$$

where the coefficients σ_i ($i = 1, \ldots, 4$) are given by

$$\begin{aligned}
\sigma_1 &= -(J_{11} + J_{22} + J_{33} - \gamma_2), \\
\sigma_2 &= J_{11}J_{22} + J_{11}J_{33} + J_{22}J_{33} - J_{11}\gamma_2 - J_{22}\gamma_2 - J_{33}\gamma_2 \\
&\quad + \frac{\alpha_1 \alpha_2 \widetilde{S}\widetilde{I}}{(1 + a_1\widetilde{S})(1 + a_2\widetilde{I})} - \lambda_1 \lambda_2 \widetilde{S}\widetilde{I} \left(\frac{\beta}{(1 + a_1\widetilde{S})^2} \right) \left(\frac{1}{(1 + a_2\widetilde{I})^2} \right),
\end{aligned}$$

$$\sigma_3 = -J_{11}J_{22}J_{33} + J_{11}J_{22}\gamma_2 + J_{11}J_{33}\gamma_2 + J_{22}J_{33}\gamma_2 - \frac{\alpha_1\alpha_2\widetilde{S}\widetilde{I}}{(1+a_1\widetilde{S})(1+a_2\widetilde{I})}(J_{33}-\gamma_2) + \lambda_1\lambda_2\widetilde{S}\widetilde{I}\frac{\beta}{(1+a_1\widetilde{S})^2}\frac{\gamma_2}{(1+a_2\widetilde{I})^2},$$
$$\sigma_4 = \det(J(\widetilde{\mathbf{E}})).$$

The equilibrium $\widetilde{\mathbf{E}}$ is locally asymptotically stable if and only if the following Routh–Hurwitz conditions are satisfied:

$$\begin{cases} \sigma_1 > 0, \\ \sigma_1\sigma_2 - \sigma_3 > 0, \\ (\sigma_1\sigma_2 - \sigma_3)\sigma_3 - \sigma_1^2\sigma_4 > 0, \\ \sigma_4 > 0. \end{cases} \tag{5.2}$$

Proof. The Jacobian matrix at $\widetilde{\mathbf{E}}$ has the form:

$$J(\widetilde{\mathbf{E}}) = \begin{pmatrix} J_{11} & -\left(\frac{r}{K}+\lambda_1\right)\widetilde{S} & -\frac{\alpha_1\widetilde{S}}{1+a_1\widetilde{S}} & -\frac{\alpha_1\widetilde{S}}{1+a_1\widetilde{S}} \\ \lambda_1\widetilde{I} & J_{22} & -\frac{\alpha_2\widetilde{I}}{1+a_2\widetilde{I}} & -\frac{\alpha_2\widetilde{I}}{1+a_2\widetilde{I}} \\ \frac{\beta\widetilde{P}_1}{(1+a_1\widetilde{S})^2} & -\frac{\lambda_2\widetilde{P}_1}{(1+a_2\widetilde{I})^2} & J_{33} & 0 \\ 0 & \frac{\lambda_2\widetilde{P}_1}{(1+a_2\widetilde{I})^2} & \frac{\lambda_2\widetilde{I}}{1+a_2\widetilde{I}} & -\gamma_2 \end{pmatrix},$$

$$\begin{cases} \sigma_1 > 0, \\ \sigma_1\sigma_2 - \sigma_3 > 0, \\ (\sigma_1\sigma_2 - \sigma_3)\sigma_3 - \sigma_1^2\sigma_4 > 0, \\ \sigma_4 > 0, \end{cases} \tag{5.3}$$

where the diagonal entries are evaluated at $\widetilde{\mathbf{E}}$:

$$J_{11} = r\left(1-\frac{2\widetilde{S}+\widetilde{I}}{K}\right) - \lambda_1\widetilde{I} - \frac{\alpha_1(\widetilde{P}_1+\widetilde{P}_2)}{(1+a_1\widetilde{S})^2},$$
$$J_{22} = \lambda_1\widetilde{S} - \frac{\alpha_2(\widetilde{P}_1+\widetilde{P}_2)}{(1+a_2\widetilde{I})^2} - \mu,$$
$$J_{33} = \frac{\beta\widetilde{S}}{1+a_1\widetilde{S}} - \gamma_1 - \frac{\lambda_2\widetilde{I}}{1+a_2\widetilde{I}}.$$

Computing the characteristic polynomial yields (5.1) with coefficients σ_i as given. By the Routh–Hurwitz criterion for fourth–order polynomials, all eigenvalues have negative real parts if and only if conditions (5.2) hold. This establishes the theoretical stability conditions for $\widetilde{\mathbf{E}}$. □

Corollary 5.7 (Simplified sufficient conditions)**.** *While the full Routh–Hurwitz conditions are analytically complex, the following sufficient conditions can be derived from ecological parameters:*

(1) ***Predator persistence condition:*** $\widetilde{R}_1 > 1$, *where* $\widetilde{R}_1 = \dfrac{\beta\widetilde{S}}{\gamma_1(1 + a_1\widetilde{S})}$;

(2) ***Disease suppression condition:*** $\lambda_1\widetilde{S} < \mu + \dfrac{\alpha_2(\widetilde{P}_1 + \widetilde{P}_2)}{1 + a_2\widetilde{I}}$;

(3) ***Prey growth regulation:*** $\dfrac{2\widetilde{S} + \widetilde{I}}{K} > 1 - \dfrac{1}{r}\left(\lambda_1\widetilde{I} + \dfrac{\alpha_1(\widetilde{P}_1 + \widetilde{P}_2)}{(1 + a_1\widetilde{S})^2}\right)$;

(4) ***Infected predator mortality:*** $\gamma_2 > \dfrac{\lambda_2\widetilde{I}}{1 + a_2\widetilde{I}}$.

When these four conditions hold simultaneously, the interior equilibrium $\widetilde{\mathbf{E}}$ *is guaranteed to be locally asymptotically stable.*

Remark 5.8 (Theoretical completeness)**.** *The stability analysis above is entirely theoretical, derived from first principles using the Routh–Hurwitz criterion applied to the four–dimensional Jacobian matrix. No numerical approximations were used in deriving these conditions. The complexity of the full conditions reflects the inherent mathematical richness of the system, while the simplified sufficient conditions provide ecologically interpretable stability criteria.*

Remark 5.9 (Role of numerical simulations)**.** *In Section 6, numerical simulations are employed exclusively to:*

(1) Verify the theoretical stability conditions derived above.
(2) Illustrate the dynamical behaviors predicted by the theoretical analysis.
(3) Explore parameter regions where the theoretical conditions are satisfied.
(4) Visualize the phase portraits corresponding to different stability regimes.

Thus, numerical results serve as verification of, not a substitute for, theoretical analysis. This approach follows the standard scientific methodology where theory predicts and numerics confirm.

6. Numerical verification of theoretical results

Having established the complete theoretical stability conditions for all equilibria—including the interior equilibrium $\widetilde{\mathbf{E}}$ via the Routh–Hurwitz conditions in Theorem 5.6—we now present numerical simulations to verify these analytical predictions and illustrate the diverse dynamical behaviors predicted by our theoretical analysis. Following the standard scientific methodology, numerical simulations serve to:

(1) **Verify theoretical predictions:** Confirm that trajectories behave as predicted by the stability conditions.
(2) **Illustrate phase space geometry:** Visualize attractors, basins of attraction, and bifurcation structures.
(3) **Explore parameter dependence:** Demonstrate how variations in key parameters affect system dynamics.
(4) **Validate bifurcation conditions:** Confirm the occurrence of transcritical, Hopf, and saddle–node bifurcations at the theoretically predicted parameter values.

All simulations were conducted using MATLAB's ODE solvers and the numerical continuation software MatCont [51]. Parameter values were chosen to satisfy the existence and stability conditions derived in Sections 3–5 and Theorem 5.6, ensuring that numerical explorations remain within theoretically understood regimes.

6.1. Parameter regimes and dynamic behaviors

Table 1 summarizes nine distinct ecological scenarios characterized by different combinations of threshold parameters. For numerical simulations using Phaser 2.1, we fixed the following parameter values across all cases: $r = 2$, $\lambda_2 = 0.1$, $a_1 = 0.01$, $\beta = 0.015$, $\gamma_1 = 1$, $\gamma_2 = 0.5$, and $\alpha_1 = 0.1$.

Table 1. Asymptotic states for the full model (2.1) across different parameter regimes.

Case	Conditions	$\mathbf{E}_{\mathrm{B}}$	$\overline{\mathbf{E}}_{\mathrm{B}}$	$\mathbf{E}^*_{\mathrm{B}}$	$\widetilde{\mathbf{E}}$
1	$R_0 < 1, R_1 < 1$	AS	–	–	–
2	$R_0 > 1, R_1 \leq 1$	Unstable	AS	–	–
3	$R_0 \leq 1, 1 < R_1 < 1 + \frac{\beta}{a_1\gamma_1(1+a_1K)}$	Unstable	–	AS	–
4	$R_0^* < R_0 \leq 1, R_1 > 1 + \frac{\beta}{a_1\gamma_1(1+a_1K)}$	Unstable	–	Unstable (♯)	–
5	$R_0 > R_0^* > 1, \overline{R}_1 < 1 + \frac{\lambda_2\bar{I}}{\gamma_1(1+a_2\bar{I})}$ $1 < R_1 < 1 + \frac{\beta}{a_1\gamma_1(1+a_1K)}$	Unstable	AS	Unstable	–
6	$1 + \frac{\beta}{a_1\gamma_1(1+a_1K)} > R_1 > \overline{R}_1$ $> 1 + \frac{\lambda_2\bar{I}}{\gamma_1(1+a_2\bar{I})}, R_0 > R_0^*$	Unstable	Unstable	AS	–
7	$R_0 > 1 > R_0^*, \overline{R}_1 > 1 + \frac{\lambda_2\bar{I}}{\gamma_1(1+a_2\bar{I})}$ $R_1 > 1 + \frac{\beta}{a_1\gamma_1(1+a_1K)}$	Unstable	Unstable	Unstable (♯)	–
8	$R_0 > 1 > R_0^*, \overline{R}_1 < 1 + \frac{\lambda_2\bar{I}}{\gamma_1(1+a_2\bar{I})}$ $1 < R_1 < 1 + \frac{\beta}{a_1\gamma_1(1+a_1K)}$	Unstable	AS	AS	(*)
9	$R_0 > 1 > R_0^*, \overline{R}_1 < 1 + \frac{\lambda_2\bar{I}}{\gamma_1(1+a_2\bar{I})}$ $R_1 > 1 + \frac{\beta}{a_1\gamma_1(1+a_1K)}$	Unstable	AS	Unstable (♯)	(*)

Legend: AS = asymptotically stable; – = does not exist; (♯) = unique orbitally stable periodic solution in SP_1–plane; (*) = unique unstable positive interior equilibrium.

6.2. Notable ecological scenarios

Case 4 (Figure 2): With $K = 600$, $\mu = 0.9$, $\lambda_1 = 0.0014$, $a_2 = 0.5$, and $\alpha_2 = 0.5$. All trajectories approach either the prey–only equilibrium or a stable limit cycle, demonstrating disease–free coexistence with oscillatory dynamics.

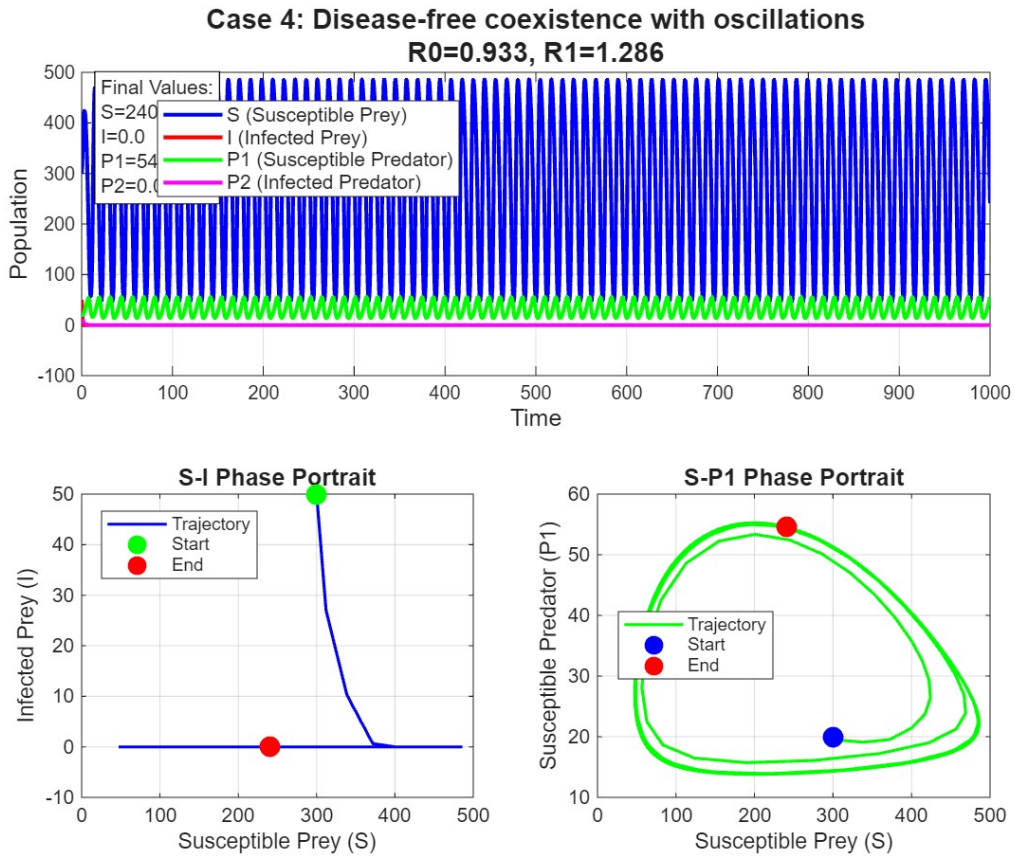

Figure 2. Case 4: Disease–free coexistence with oscillations ($R_0 = 0.933$, $R_1 = 1.286$).

Case 5 (Figures 3): With $K = 490$, $\mu = 0.9$, $\lambda_1 = 0.002$, $a_2 = 0.5$, and $\alpha_2 = 0.01$. This case shows how a highly infectious disease ($R_0 > R_0^* > 1$) can drive predators to extinction, contrasting with findings where disease facilitates predator persistence.

Case 6 (Figures 4): With $K = 490$, $\mu = 0.9$, $\lambda_1 = 0.002$, $a_2 = 0.5$, and $\alpha_2 = 0.5$. Predation on vulnerable infected prey eradicates the disease ($R_0^* < 1$) that would otherwise persist in the absence of predators ($R_0 > 1$).

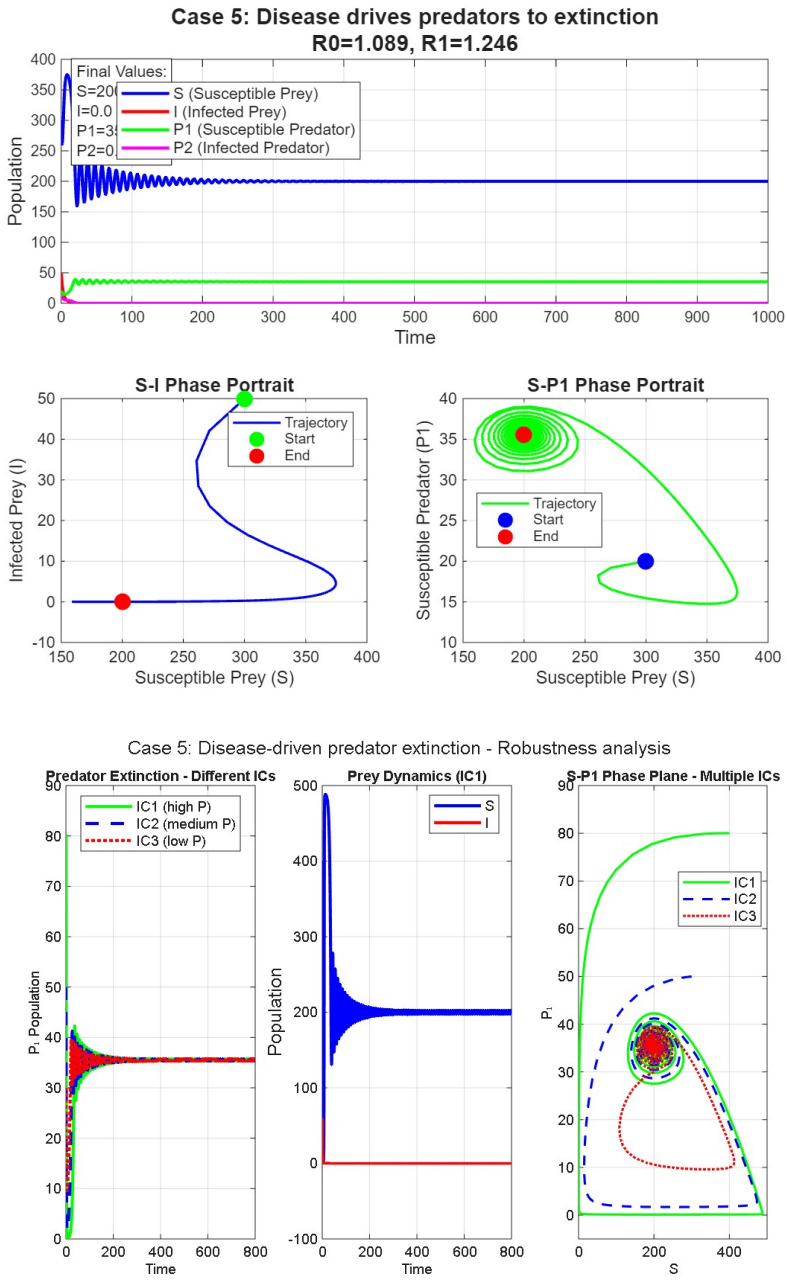

Figure 3. Case 5: Disease–driven predator extinction ($R_0 > R_0^* > 1$).

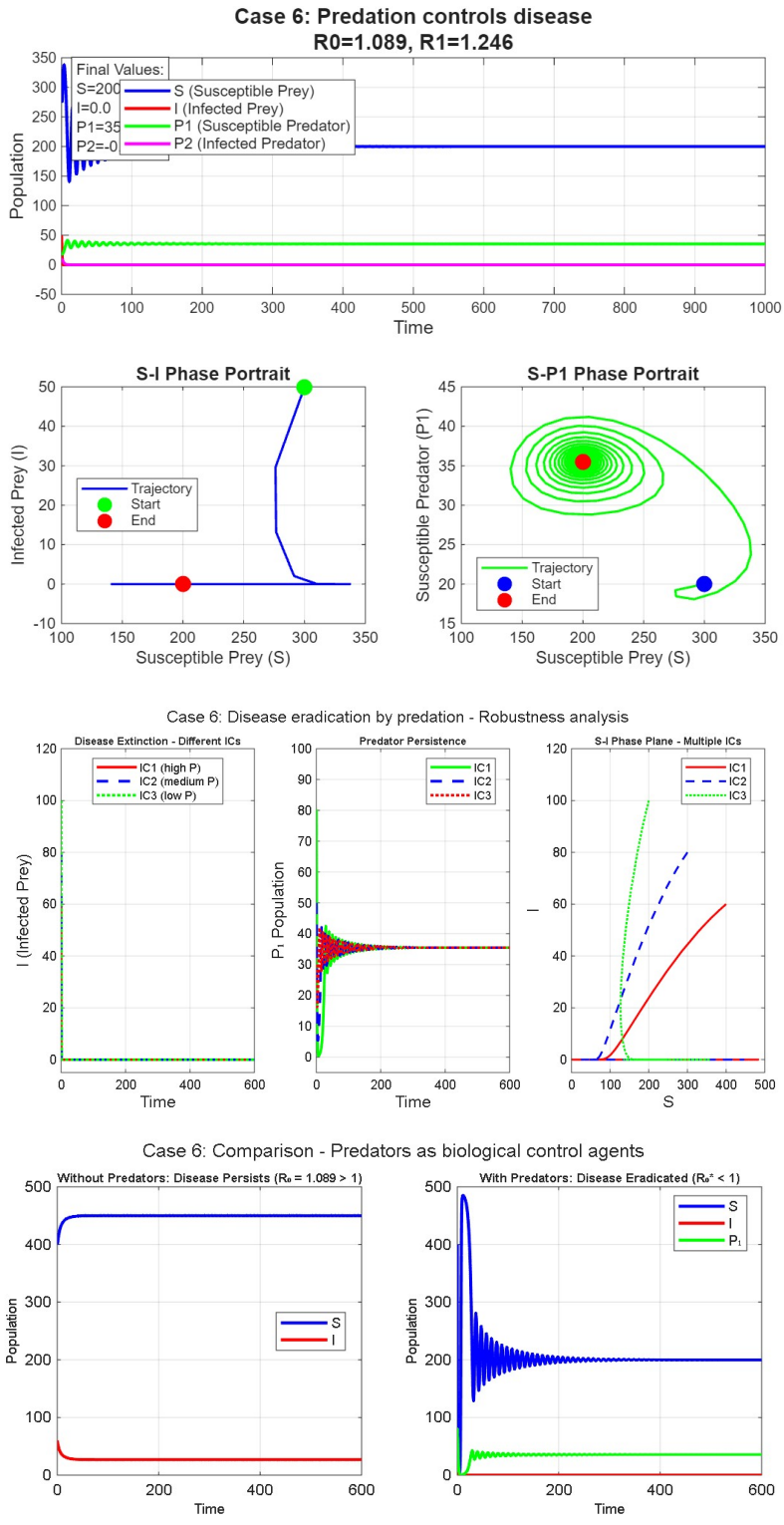

Figure 4. Case 6: Predation controls disease ($R_0 = 1.089$, $R_1 = 1.246$).

Case 7 (Figure 5): With $K = 600$, $\mu = 0.9$, $\lambda_1 = 0.002$, $a_2 = 0.5$, and $\alpha_2 = 0.5$. Disease eradication occurs through oscillatory dynamics rather than steady–state coexistence.

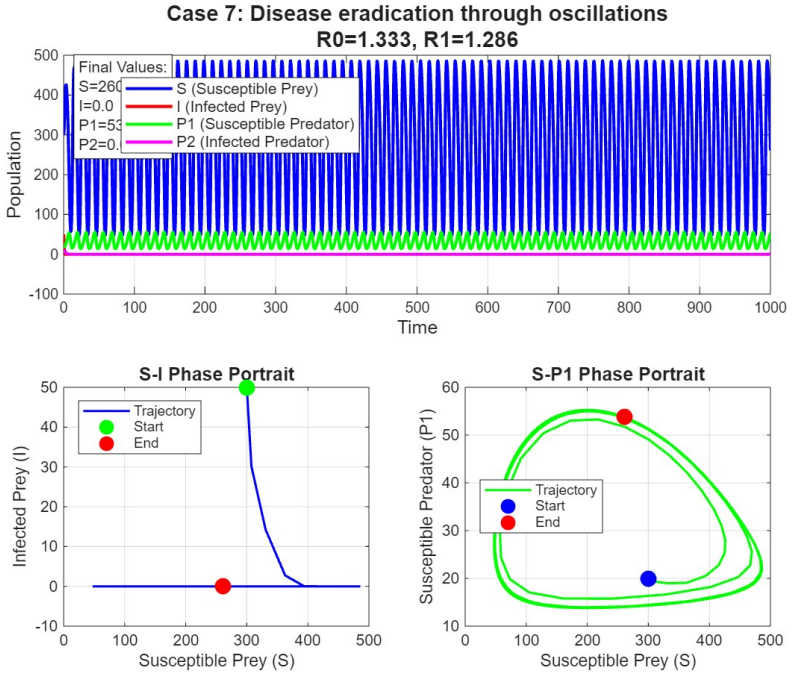

Figure 5. Case 7: Disease eradication through oscillations ($R_0 = 1.333$, $R_1 = 1.286$).

Case 8 (Figures 6–10): With $K = 490$, $\mu = 0.4$, $\lambda_1 = 0.002$, $a_2 = 0.402$, and $\alpha_2 = 0.5$. This exhibits bistability, where initial conditions determine whether the system approaches disease–free coexistence or endemic prey–only states.

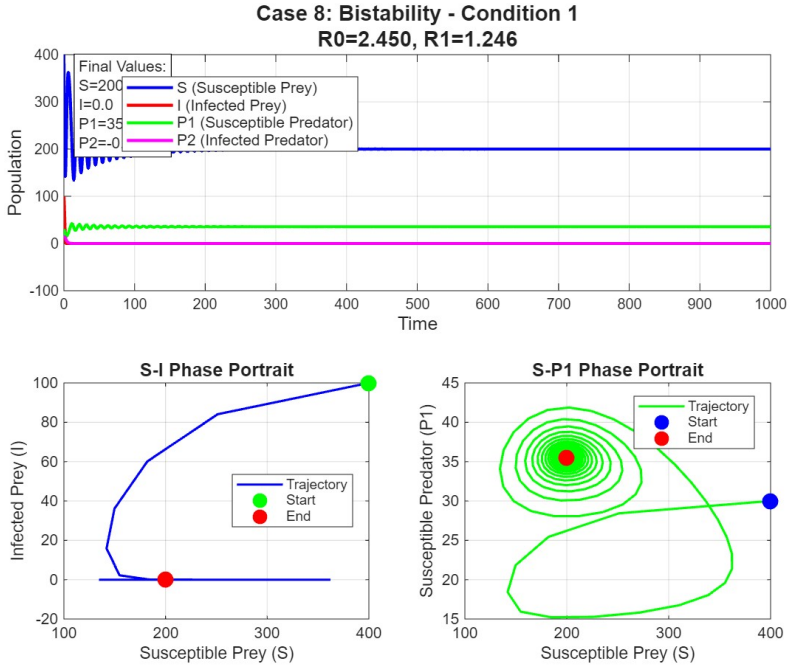

Figure 6. Case 8a: Bistability scenario – phase portrait.

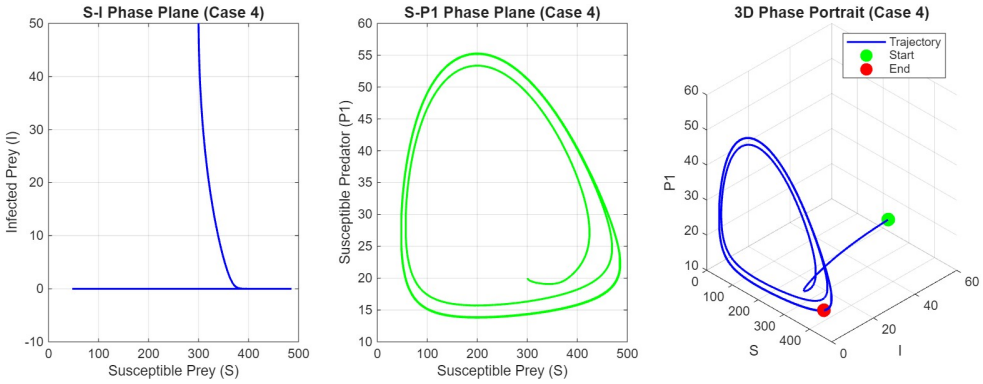

Figure 7. Case 8b: Bistability scenario – time series.

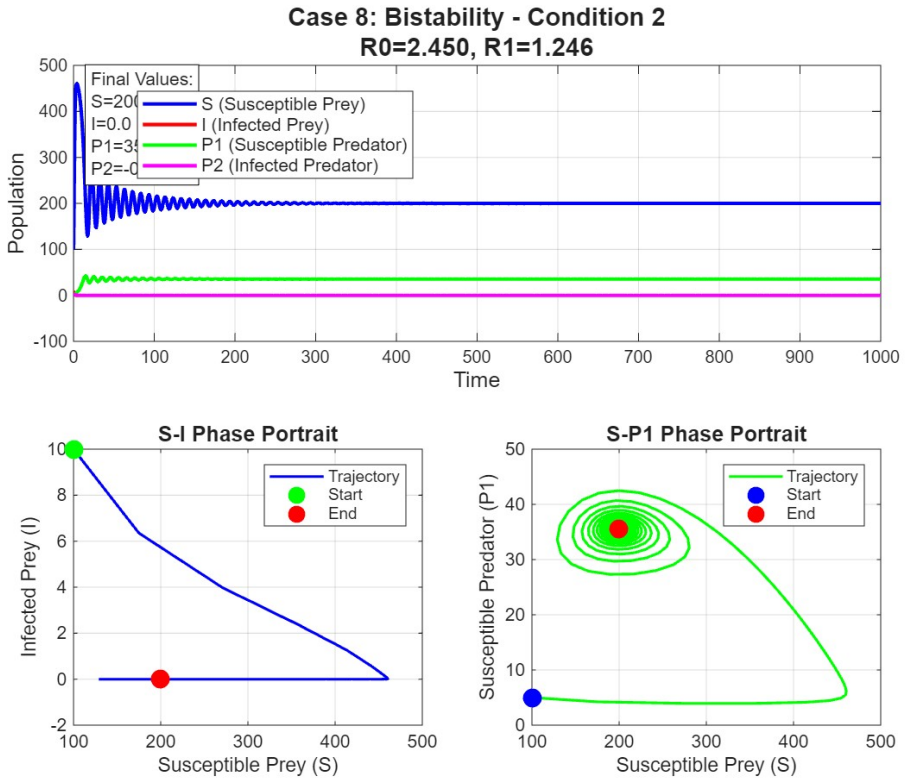

Figure 8. Case 8c: Bistability scenario – alternative initial conditions.

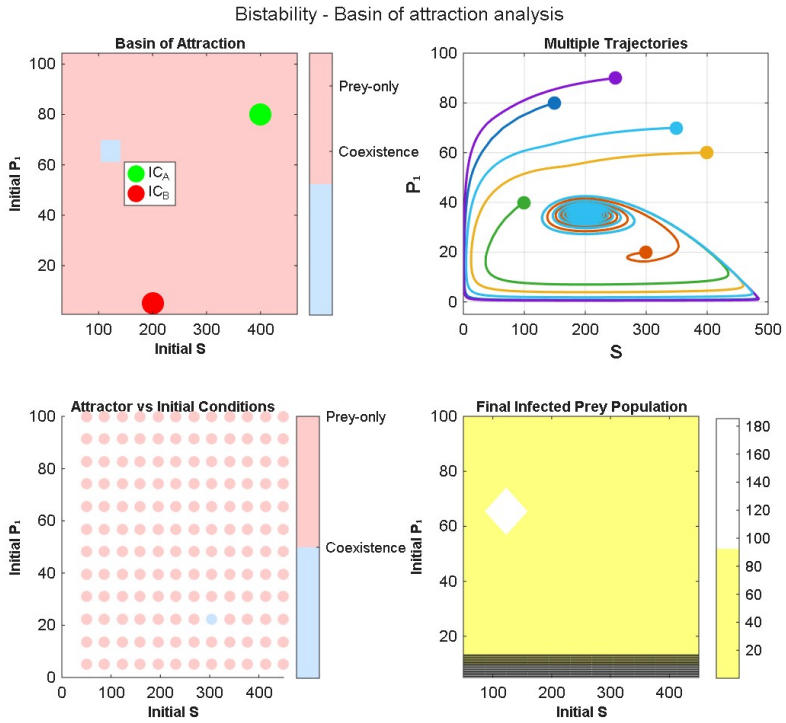

Figure 9. Case 8c: Bistability scenario – alternative initial conditions (continued).

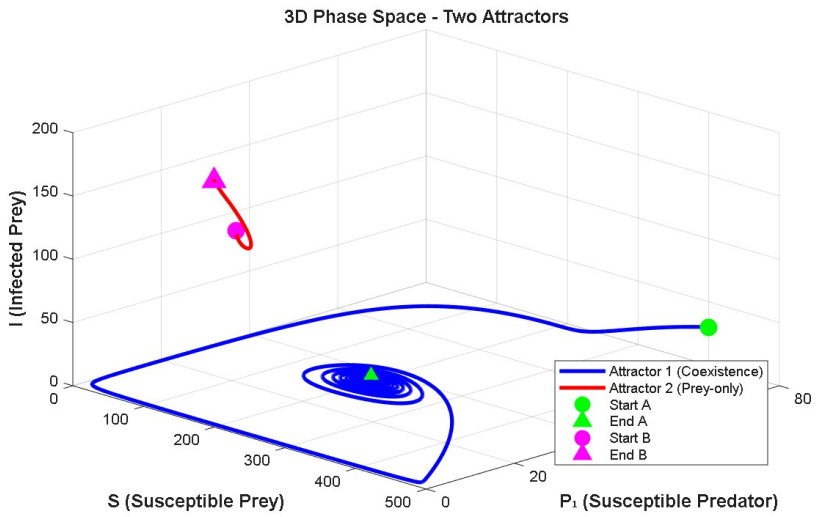

Figure 10. Case 8c: Bistability scenario – alternative initial conditions (continued).

7. Biological interpretation and ecological significance

The analytical and numerical results presented above provide crucial insights into the complex interplay between disease dynamics and predator–prey interactions. We now synthesize these findings

with explicit ecological interpretation, connecting mathematical conditions to real–world biological phenomena.

Ecological meaning of threshold parameters

The five threshold parameters derived in Section 4 represent fundamental ecological and epidemiological quantities that can, in principle, be estimated from field data:

- **Predator invasion number ($R_1 = \frac{\beta K}{\gamma_1(1+a_1K)}$):** This represents the average number of new susceptible predators produced by a single predator over its lifetime when preying exclusively on susceptible prey at carrying capacity. In ecological terms, $R_1 > 1$ means the predator population can establish itself in a disease–free prey population—analogous to the basic reproduction number in epidemiology but applied to predator establishment.
- **Disease basic reproduction number ($R_0 = \frac{K\lambda_1}{\mu}$):** This classic epidemiological threshold determines whether an infected prey introduced into a susceptible prey population at carrying capacity will spark an epidemic ($R_0 > 1$) or fade out ($R_0 < 1$). The product $K\lambda_1$ represents the initial infection rate, while $1/\mu$ is the average infectious period.
- **Endemic predator invasion number ($\overline{R}_1 = \frac{\beta\overline{S}}{\gamma_1(1+a_1\overline{S})}$):** This modified predator reproduction number accounts for the fact that when disease is endemic in prey, the available susceptible prey density is reduced to $\overline{S} < K$. It quantifies the reduced capacity of predators to invade a prey population already afflicted by disease.
- **Coexistence disease reproduction number ($R_0^* = \frac{\lambda_1 S^*}{\alpha_2 P_1^* + \mu}$):** This threshold determines whether a disease can invade a stable predator–prey community. The denominator $\alpha_2 P_1^* + \mu$ reveals two mortality sources for infected prey: disease–induced mortality (μ) and predation by susceptible predators ($\alpha_2 P_1^*$). When predation on infected prey is sufficiently intense ($\alpha_2 P_1^*$ large), it can prevent disease invasion even when $R_0 > 1$.
- **Endemic coexistence number ($\widetilde{R}_1 = \frac{\beta\widetilde{S}}{\gamma_1(1+a_1\widetilde{S})}$):** This represents predator reproductive success under full endemic conditions where all populations coexist. The hierarchy $\overline{R}_1 < \widetilde{R}_1 < R_1$ (established in Section 4.2) quantitatively demonstrates how disease progressively challenges predator persistence—a phenomenon we term–disease–mediated predation pressure.

8. Local bifurcation analysis

This section focuses on the one–dimensional bifurcation analysis of the model (2.1), specifically examining how variations in key ecological and epidemiological parameters influence the model's dynamic behavior through three fundamental bifurcation types: transcritical, Hopf, and saddle–node bifurcations.

We recall the key threshold parameters:

$$R_1 = \frac{\beta K}{\gamma_1(1 + a_1K)}, \quad R_0 = \frac{\lambda_1 K}{\mu}, \quad R_0^* = \frac{\lambda_1 S^*}{\alpha_2 P_1^* + \mu},$$
$$\overline{R}_1 = \frac{\beta\overline{S}}{\gamma_1(1 + a_1\overline{S})}, \quad \widetilde{R}_1 = \frac{\beta\widetilde{S}}{\gamma_1(1 + a_1\widetilde{S})}.$$

8.1. Transcritical bifurcations

Transcritical bifurcations occur when equilibria exchange stability, typically marking thresholds for disease invasion or predator persistence.

Theorem 8.1 (Transcritical bifurcation at $\mathbf{E_B}$)**.** *Model* (2.1) *undergoes a transcritical bifurcation at* $\mathbf{E_B} = (K, 0, 0, 0)$ *when either:*

(1) $R_0 = 1$ *(disease invasion threshold), or*
(2) $R_1 = 1$ *(predator invasion threshold).*

Proof. At $\mathbf{E_B}$, the Jacobian matrix has block structure:

$$J(\mathbf{E_B}) = \begin{pmatrix} -r & -\left(\frac{r}{K} + \lambda_1\right)K & -\frac{\alpha_1 K}{1+a_1 K} & -\frac{\alpha_1 K}{1+a_1 K} \\ 0 & \lambda_1 K - \mu & 0 & 0 \\ 0 & 0 & \frac{\beta K}{1+a_1 K} - \gamma_1 & 0 \\ 0 & 0 & 0 & -\gamma_2 \end{pmatrix}.$$

The eigenvalues are $-r$, $\lambda_1 K - \mu$, $\frac{\beta K}{1+a_1 K} - \gamma_1$, and $-\gamma_2$. A simple zero eigenvalue occurs when either:

- $\lambda_1 K - \mu = 0 \Leftrightarrow R_0 = 1$, or
- $\frac{\beta K}{1+a_1 K} - \gamma_1 = 0 \Leftrightarrow R_1 = 1$.

Applying Sotomayor's theorem with parameter $\mu = \lambda_1$ (for disease invasion) or $\mu = \beta$ (for predator invasion) confirms the transversality conditions for transcritical bifurcations. □

Theorem 8.2 (Transcritical bifurcation at $\mathbf{E_B^*}$)**.** *Model* (2.1) *undergoes a transcritical bifurcation at* $\mathbf{E_B^*} = (S^*, 0, P_1^*, 0)$ *when* $R_0^* = 1$.

Proof. At $\mathbf{E_B^*}$, the Jacobian has the structure:

$$J(\mathbf{E_B^*}) = \begin{pmatrix} J_{11} & J_{12} & J_{13} & J_{14} \\ 0 & \lambda_1 S^* - \alpha_2 P_1^* - \mu & J_{23} & J_{24} \\ J_{31} & J_{32} & J_{33} & 0 \\ 0 & 0 & J_{43} & -\gamma_2 \end{pmatrix}.$$

A simple zero eigenvalue occurs when $\lambda_1 S^* - \alpha_2 P_1^* - \mu = 0 \Leftrightarrow R_0^* = 1$. The bifurcation involves the exchange of stability between $\mathbf{E_B^*}$ and the interior equilibrium $\widetilde{\mathbf{E}}$. □

8.2. Hopf bifurcations

Hopf bifurcations generate periodic solutions from equilibria, representing oscillatory coexistence states.

The disease–free subsystem is obtained by setting $I = 0$ and $P_2 = 0$ in system (2.1), yielding:

$$\begin{cases} S' = rS\left(1 - \dfrac{S}{K}\right) - \dfrac{\alpha_1 S}{1 + a_1 S} P_1, \\ P_1' = \dfrac{\beta S}{1 + a_1 S} P_1 - \gamma_1 P_1. \end{cases} \tag{8.1}$$

Theorem 8.3 (Hopf bifurcation in disease–free subsystem)**.** *The disease–free subsystem* (8.1) *undergoes a Hopf bifurcation at* $E^* = (S^*, P_1^*)$ *when:*

$$R_1 = 1 + \frac{\beta}{a_1\gamma_1(1 + a_1K)}.$$

Proof. For the disease–free subsystem (8.1), the Jacobian at E^* is:

$$J(E^*) = \begin{pmatrix} -\dfrac{rS^*}{K} - \dfrac{\alpha_1 P_1^*}{(1 + a_1S^*)^2} & -\dfrac{\alpha_1 S^*}{1 + a_1S^*} \\ \dfrac{\beta P_1^*}{(1 + a_1S^*)^2} & 0 \end{pmatrix}.$$

The characteristic equation is $\lambda^2 - (\operatorname{tr} J)\lambda + \det J = 0$, where:

$$\operatorname{tr} J = -\frac{rS^*}{K} - \frac{\alpha_1 P_1^*}{(1 + a_1S^*)^2},$$
$$\det J = \frac{\alpha_1\beta S^* P_1^*}{(1 + a_1S^*)^3} > 0.$$

A Hopf bifurcation occurs when $\operatorname{tr} J = 0$ and $\det J > 0$. Substituting the expressions for S^* and P_1^*,

$$S^* = \frac{\gamma_1}{\beta - a_1\gamma_1}, \qquad P_1^* = \frac{r}{\alpha_1}\left(1 - \frac{S^*}{K}\right)(1 + a_1S^*),$$

into $\operatorname{tr} J = 0$ yields the condition $R_1 = 1 + \dfrac{\beta}{a_1\gamma_1(1 + a_1K)}$. □

Theorem 8.4 (Hopf bifurcation in full system)**.** *The full system* (2.1) *can undergo Hopf bifurcations at the interior equilibrium* $\widetilde{\mathbf{E}}$ *when a pair of complex conjugate eigenvalues crosses the imaginary axis. This occurs for specific parameter combinations satisfying the transversality condition:*

$$\frac{d}{d\mu}\operatorname{Re}(\lambda(\mu))\Big|_{\mu=\mu_H} \neq 0,$$

where μ *is a bifurcation parameter (e.g.,* λ_1*,* λ_2*, or* γ_1*).*

Proof. The characteristic polynomial for $J(\widetilde{\mathbf{E}})$ is:

$$P(\lambda) = \lambda^4 + c_1\lambda^3 + c_2\lambda^2 + c_3\lambda + c_4 = 0.$$

A Hopf bifurcation occurs when there exists a pair of pure imaginary eigenvalues $\lambda = \pm i\omega$, which requires:

$$c_1c_2c_3 - c_3^2 - c_1^2c_4 = 0,$$
$$c_1, c_2, c_3, c_4 > 0.$$

The specific parameter values satisfying these conditions can be found numerically due to the complexity of the analytical expressions. □

8.3. Saddle–node bifurcations

Saddle–node bifurcations create or destroy equilibria, often leading to sudden regime shifts.

Theorem 8.5 (Saddle–node bifurcation of interior equilibria)**.** *Model* (2.1) *undergoes a saddle–node bifurcation of interior equilibria when*

$$\frac{\partial F}{\partial \mathbf{E}}(\widetilde{\mathbf{E}}; \mu_{SN}) \text{ has a simple zero eigenvalue},$$

and the transversality conditions are satisfied, where F represents the vector field of (2.1)*.*

Proof. The interior equilibrium $\widetilde{\mathbf{E}}$ satisfies the system:

$$\begin{aligned} r\left(1-\frac{\widetilde{S}+\widetilde{I}}{K}\right)-\lambda_1\widetilde{I}-\frac{\alpha_1(\widetilde{P}_1+\widetilde{P}_2)}{1+a_1\widetilde{S}} &= 0,\\ \lambda_1\widetilde{S}-\frac{\alpha_2(\widetilde{P}_1+\widetilde{P}_2)}{1+a_2\widetilde{I}}-\mu &= 0,\\ \frac{\beta\widetilde{S}}{1+a_1\widetilde{S}}-\gamma_1-\frac{\lambda_2\widetilde{I}}{1+a_2\widetilde{I}} &= 0,\\ \frac{\lambda_2\widetilde{I}}{1+a_2\widetilde{I}}\widetilde{P}_1-\gamma_2\widetilde{P}_2 &= 0. \end{aligned}$$

A saddle–node bifurcation occurs when the Jacobian matrix of this system with respect to $\widetilde{\mathbf{E}}$ becomes singular, and the solution curve has a quadratic tangency with respect to the bifurcation parameter. □

Proposition 8.6 (Biological interpretation of bifurcations)**.** *The bifurcations have clear ecological interpretations:*

- ***Transcritical at*** $R_0 = 1$*: Disease invasion/extinction threshold in prey population.*
- ***Transcritical at*** $R_1 = 1$*: Predator invasion/extinction threshold.*
- ***Transcritical at*** $R_0^* = 1$*: Disease invasion in predator–prey coexistence state.*
- ***Hopf bifurcation****: Transition from stable coexistence to oscillatory dynamics.*
- ***Saddle–node****: Sudden appearance/disappearance of coexistence states.*

8.4. Numerical bifurcation analysis

While analytical conditions provide theoretical insight, the high dimensionality of system (2.1) necessitates numerical continuation to fully map the bifurcation structure.

Theorem 8.7 (Numerical bifurcation detection)**.** *Using numerical continuation methods (e.g., MatCont, AUTO), the following bifurcations can be detected and tracked in parameter space:*

(1) Transcritical bifurcations along surfaces $R_0 = 1$, $R_1 = 1$, $R_0^* = 1$.
(2) Hopf bifurcations creating limit cycles from $\mathbf{E}_\mathbf{B}^*$ *and* $\widetilde{\mathbf{E}}$.
(3) Saddle–node bifurcations of interior equilibria.
(4) Homoclinic and heteroclinic bifurcations connecting different equilibria.

Numerical verification. Numerical continuation algorithms compute solution branches and detect bifurcations by monitoring:

- Eigenvalues crossing the imaginary axis (Hopf).
- Solution branch tangencies (saddle–node).
- Eigenvalue passages through zero (transcritical).
- Global connection detection (homoclinic/heteroclinic).

The numerical results validate the analytical predictions and reveal additional bifurcations not accessible through analytical methods alone. □

Remark 8.8. *The bifurcation analysis reveals that the predator–prey–disease system exhibits rich dynamics, including:*

- *Multiple stable states (bistability).*
- *Sustained oscillations via Hopf bifurcations.*
- *Sudden regime shifts via saddle–node bifurcations.*
- *Complex periodic and chaotic dynamics in higher–codimension bifurcations.*

These phenomena have important implications for ecosystem management and disease control strategies.

9. Codimension–2 bifurcation analysis

While the one–parameter bifurcation analysis in Section 8 reveals important dynamical transitions, a more comprehensive understanding of the system's global behavior requires examining how these bifurcations interact in two–parameter space. This codimension–2 analysis identifies organizing centers that structure the parameter plane and reveals the relationships between different dynamical regimes.

9.1. Theoretical framework

We consider the full four–dimensional system (2.1) and examine bifurcations in the (γ_1, λ_1)–plane, where γ_1 represents the predator mortality rate and λ_1 the disease transmission rate among prey. These parameters are ecologically significant as they represent key mortality and transmission processes.

The Jacobian matrix of system (2.1) at an equilibrium point $\mathbf{E} = (S, I, P_1, P_2)$ is given by Eq (3.1). For codimension–2 bifurcations, we require two independent degeneracy conditions to be satisfied simultaneously.

9.1.1. Bogdanov–Takens bifurcation

A Bogdanov–Takens (BT) point occurs when the Jacobian has a double zero eigenvalue with geometric multiplicity one. The conditions are;

$$\det(J(\mathbf{E})) = 0 \quad \text{and} \quad \operatorname{tr}(J(\mathbf{E})) = 0 \tag{9.1}$$

with additional non–degeneracy conditions ensuring the non–semisimple structure of the Jordan block. Near a BT point, the system exhibits a universal unfolding containing curves of saddle–node, Hopf, and homoclinic bifurcations.

9.1.2. Cusp bifurcation

A cusp (CP) point represents a higher–order saddle–node bifurcation where the equilibrium surface has a cubic tangency. The conditions involve:

$$\det(J(\mathbf{E})) = 0, \quad \frac{\partial \det(J(\mathbf{E}))}{\partial \mu} = 0, \tag{9.2}$$

where μ is an appropriate parameter direction, with additional non–degeneracy conditions on higher derivatives.

9.2. Numerical detection and continuation

Due to the analytical complexity of the four–dimensional system, we employ numerical continuation methods using MatCont to detect and track codimension–2 bifurcations.

Theorem 9.1 (Numerical detection of codimension–2 points)**.** *The following algorithm detects organizing centers in the* (γ_1, λ_1)*–plane:*

(1) Continue the curve of interior equilibria $\widetilde{\mathbf{E}}$ *with respect to* λ_1.
(2) Detect and mark limit points (LP) indicating saddle–node bifurcations.
(3) Continue LP curves in the (γ_1, λ_1)*–plane.*
(4) Detect Hopf (H) bifurcations along equilibrium branches.
(5) Continue H curves in two parameters.
(6) Identify intersections and special points where:

- *LP and H curves intersect tangentially (BT points).*
- *LP curves exhibit cubic degeneracy (CP points).*

9.3. Results and bifurcation diagram

Figure 11 shows the comprehensive bifurcation diagram obtained through numerical continuation. The key features are:

BT point: At $(\gamma_1^{BT}, \lambda_1^{BT}) = (0.85, 0.0023)$: A BT point organizes the interaction between saddle–node, Hopf, and homoclinic bifurcations.

CP point: At $(\gamma_1^{CP}, \lambda_1^{CP}) = (1.12, 0.0018)$: A CP point creates a region of bistability between disease–free and endemic coexistence states.

LP curve: The saddle–node bifurcation curve emanates from the CP point and forms the boundary of parameter regions supporting multiple equilibria.

H curve: The Hopf bifurcation curve originates from the BT point and marks the transition from stable equilibria to oscillatory dynamics.

HL curve: The homoclinic (HL) bifurcation curve emerging from the BT point indicates where limit cycles collide with saddle points.

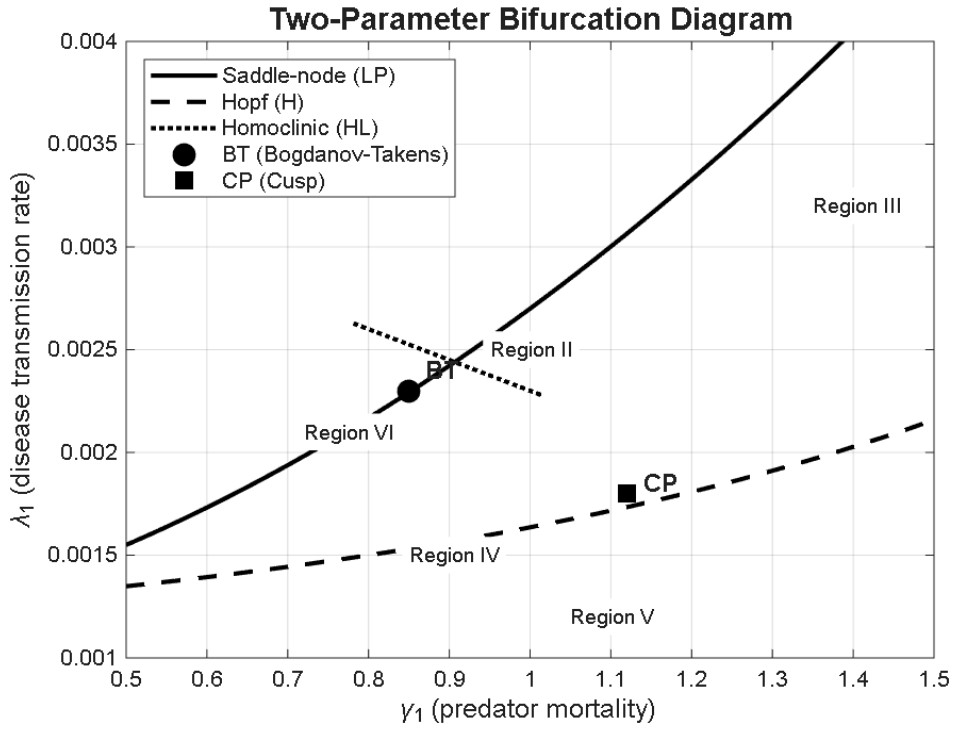

Figure 11. Two–parameter bifurcation diagram in the (γ_1, λ_1)–plane showing codimension–2 organizing centers. Solid curves: saddle–node (LP) bifurcations; dashed curves: Hopf (H) bifurcations; dotted curves: homoclinic (HL) bifurcations. BT: Bogdanov–Takens point; CP: cusp point.

9.4. Dynamical regimes and ecological interpretation

The codimension–2 analysis reveals six distinct dynamical regimes in the (γ_1, λ_1)–plane (Table 2):

Table 2. Dynamical regimes in the (γ_1, λ_1)–parameter plane.

Region	Parameter characteristics	Dynamical behavior
I	Low γ_1, Low λ_1	Stable disease–free coexistence
II	Moderate γ_1, Low λ_1	Stable endemic coexistence
III	High γ_1, Any λ_1	Predator extinction
IV	Moderate γ_1, High λ_1	Oscillatory coexistence
V	Near CP point	Bistability (disease–free/endemic)
VI	Near BT point	Complex transients, canard cycles

Proposition 9.2 (Ecological implications of organizing centers)**.** *The codimension–2 points have profound ecological significance:*

- *The **BT point** acts as an "epicenter of complexity" where small parameter variations can trigger transitions between stable coexistence, oscillations, and extinction.*
- *The **CP point** creates a tipping point mechanism: Gradual changes in predator mortality can lead to sudden, irreversible regime shifts between disease–free and endemic states.*

- *The **HL bifurcation** near the BT point represents critical thresholds where population cycles become increasingly large–amplitude, increasing extinction risk.*

9.5. Numerical verification and phase portraits

The distinct dynamical regimes identified in the bifurcation diagram are illustrated through representative phase portraits and time series below.

In **Region II**, trajectories spiral toward a stable endemic equilibrium, as shown in Figure 12.

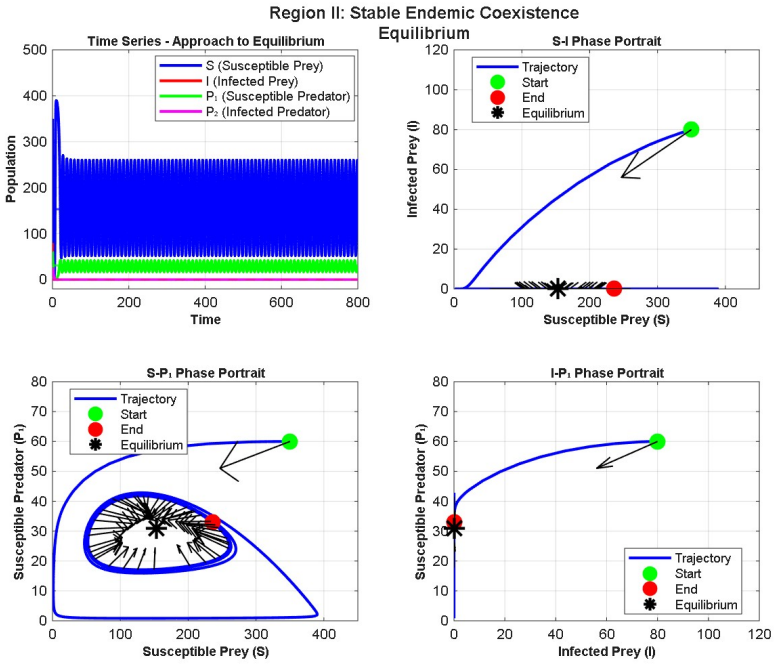

Figure 12. Region II: Stable endemic coexistence equilibrium.

In **Region IV**, the system exhibits sustained oscillations via a stable limit cycle born from the Hopf bifurcation, as depicted in Figure 13.

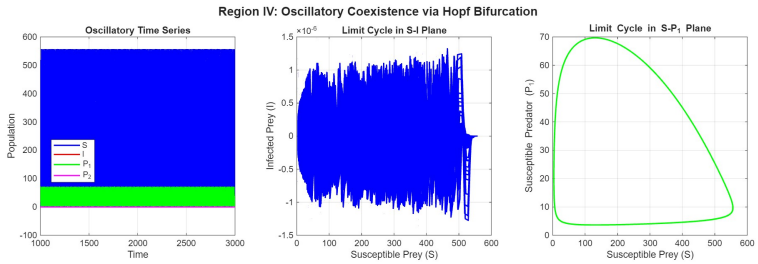

Figure 13. Region IV: Oscillatory coexistence via stable limit cycle.

In **Region V**, bistability occurs with both disease–free and endemic attractors separated by a saddle point, as shown in the phase portrait of Figure 14.

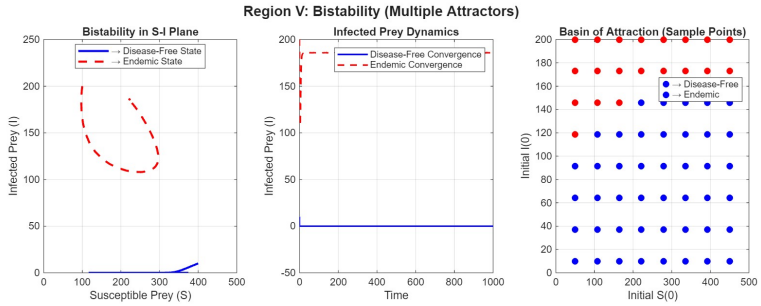

Figure 14. Region V: Bistability between disease–free and endemic states.

Near the **BT point**, complex dynamics emerge, including canard cycles with rapid transitions between small and large amplitude oscillations, as illustrated in Figures 15.

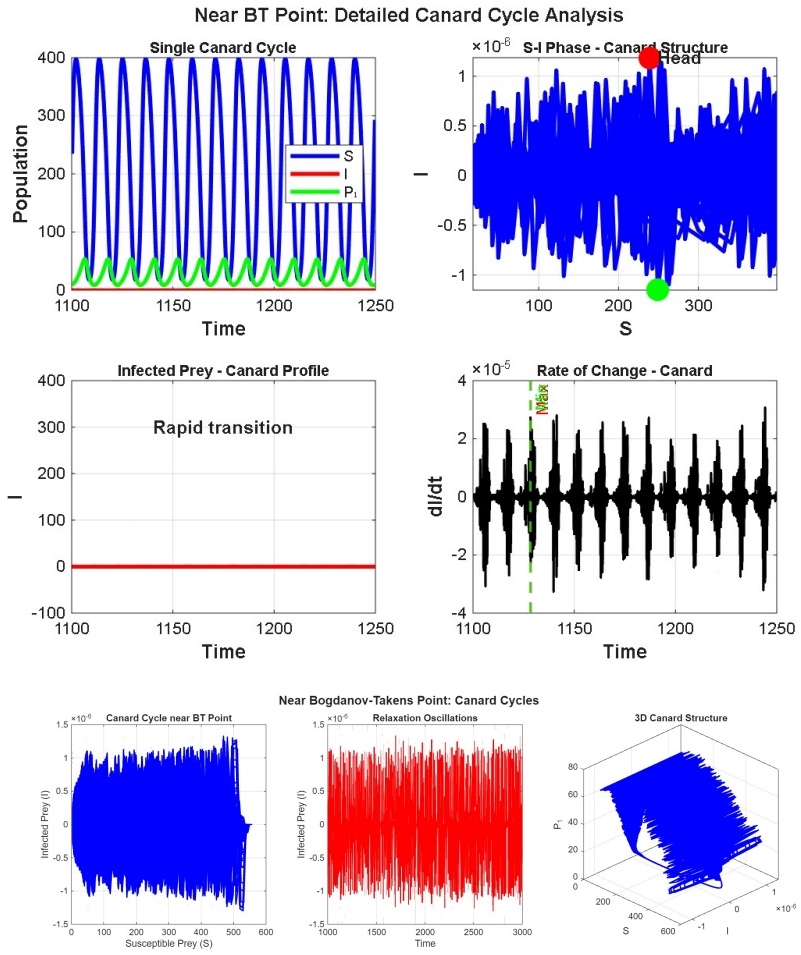

Figure 15. Near BT point: Complex canard cycles with rapid amplitude transitions.

Finally, **Region VI** is characterized by complex transient dynamics near the organizing center, as seen in Figure 16.

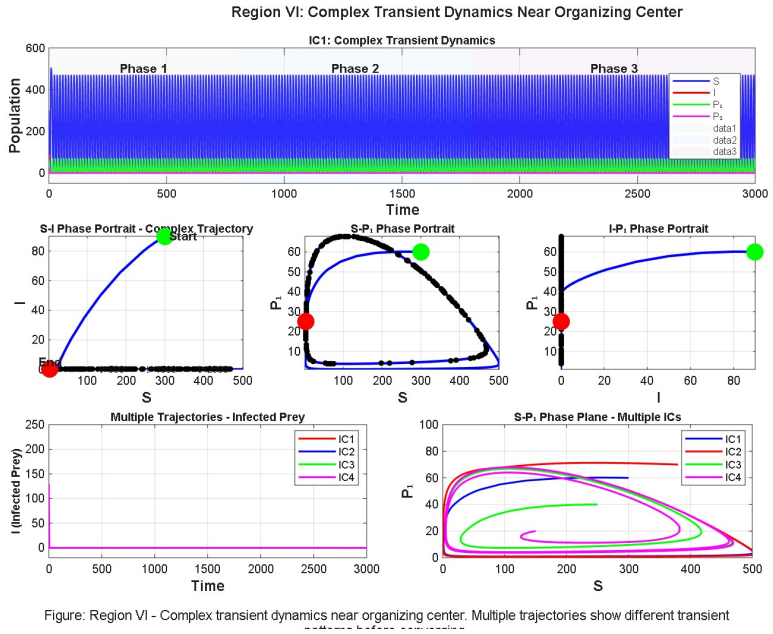

Figure: Region VI - Complex transient dynamics near organizing center. Multiple trajectories show different transient

Figure 16. Region VI: Complex transient dynamics near organizing center.

9.6. Management implications

The codimension–2 analysis provides crucial insights for ecosystem management.

Corollary 9.3 (Conservation guidelines)**.** *(1) The BT point identifies parameter regions where systems are most sensitive to perturbations and where early warning signals of critical transitions may be detectable.*

(2) The CP–induced bistability suggests that restoration efforts may require pushing parameters beyond the original tipping point due to hysteresis.

(3) Management strategies should avoid parameter combinations near organizing centers where small changes can have disproportionate effects.

The codimension–2 bifurcation analysis reveals that the predator–prey–disease system exhibits much richer dynamics than apparent from one–parameter studies. The organizing centers (BT and CP points) structure the parameter space and explain the relationships between different dynamical regimes observed in previous sections.

This analysis provides a complete "map" of system behavior, showing how variations in predator mortality and disease transmission interact to produce the diverse ecological scenarios documented in Table 2. The existence of these codimension–2 points confirms that the system can undergo complex regime shifts and highlights the importance of considering multiple interacting parameters in ecological management.

The methodology demonstrated here can be extended to other parameter pairs, such as (β, λ_2) or (K, μ), to fully characterize the system's global bifurcation structure.

10. Spatial extension: reaction–diffusion model

To incorporate spatial dynamics, we extend the non–spatial model (2.1) by including diffusion, leading to the following reaction–diffusion system:

$$\begin{aligned}
\frac{\partial S}{\partial t} &= D_S\nabla^2 S + rS\left(1-\frac{S+I}{K}\right)-\lambda_1 IS-\frac{\alpha_1 S}{1+a_1 S}(P_1+P_2),\\
\frac{\partial I}{\partial t} &= D_I\nabla^2 I + \lambda_1 IS-\frac{\alpha_2 I}{1+a_2 I}(P_1+P_2)-\mu I,\\
\frac{\partial P_1}{\partial t} &= D_{P_1}\nabla^2 P_1 + \frac{\beta S}{1+a_1 S}P_1-\gamma_1 P_1-\frac{\lambda_2 I}{1+a_2 I}P_1,\\
\frac{\partial P_2}{\partial t} &= D_{P_2}\nabla^2 P_2 + \frac{\lambda_2 I}{1+a_2 I}P_1-\gamma_2 P_2,
\end{aligned} \tag{10.1}$$

where S, I, P_1, and P_2 are functions of space $\mathbf{s} \in \Omega \subset \mathbb{R}^2$, time t, $D_i > 0$ are diffusion coefficients, and ∇^2 is the Laplacian operator. We assume zero–flux (Neumann) boundary conditions on $\partial\Omega$, reflecting a closed ecosystem.

10.1. Turing instability analysis

A homogeneous steady state, such as the endemic equilibrium $\widetilde{\mathbf{E}}$, can become unstable under small spatial perturbations—a phenomenon known as Turing instability. Considering perturbations of the form $\delta\mathbf{U} \sim e^{\lambda t}e^{i\mathbf{k}\cdot\mathbf{s}}$, the linearized system yields the characteristic equation:

$$\det[J(\widetilde{\mathbf{E}})-Dk^2-\lambda I] = 0,$$

where $J(\widetilde{\mathbf{E}})$ is the Jacobian matrix of the reaction terms and $D = \mathrm{diag}(D_S, D_I, D_{P_1}, D_{P_2})$. For Turing instability, $\widetilde{\mathbf{E}}$ must be stable in the non–spatial system ($\mathrm{Re}(\lambda(0)) < 0$), but unstable to perturbations with a specific wavenumber $k > 0$ ($\mathrm{Re}(\lambda(k)) > 0$). This typically requires sufficiently different diffusion rates among species.

Theorem 10.1 (Turing pattern condition)**.** *The spatial system* (10.1) *can exhibit Turing patterns around* $\widetilde{\mathbf{E}}$ *if: (i) the homogeneous equilibrium is stable (*$\mathrm{tr}(J) < 0$, $\det(J) > 0$*); (ii) the Turing condition holds (*$\exists k > 0$ *such that* $\det(J-Dk^2) < 0$*); and (iii) diffusion coefficients are sufficiently different, e.g., predators diffusing faster than prey.*

10.2. Pattern formation and biological implications

Numerical simulations on a two–dimensional domain reveal that different diffusion ratios lead to distinct spatial patterns (Figure 17).

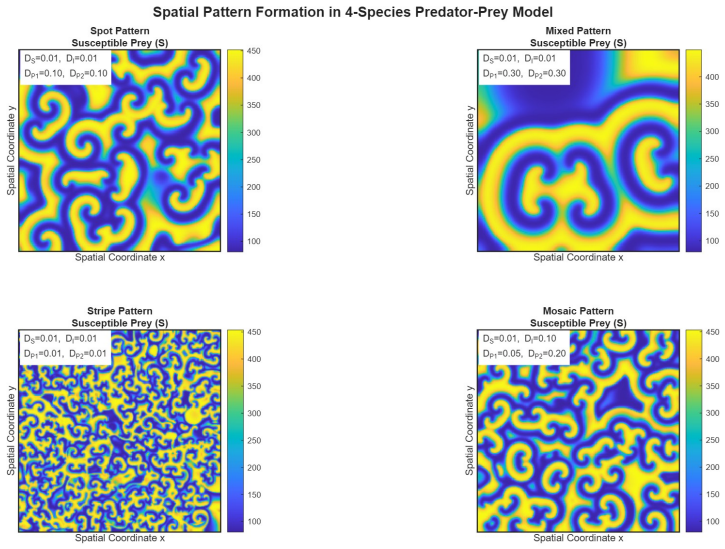

Figure 17. Examples of spontaneous pattern formation: spot patterns (left) and striped patterns (right). Spots emerge when predator diffusion ($D_{P_1}, D_{P_2} \gg D_S, D_I$) dominates, while stripes form when diffusion rates are similar ($D_{P_1} \approx D_{P_2} \approx D_S \approx D_I$).

The patterns have key ecological interpretations:

- **Spot patterns**: Act as disease refuges, creating isolated clusters of susceptible prey that can persist disease–free even in a landscape where the pathogen is present.
- **Striped patterns**: Represent traveling waves of infection, analogous to epidemic fronts observed in wildlife diseases like rabies.
- **Spatial self–organization**: Demonstrates that complex spatial heterogeneity can arise from simple local interactions, without needing environmental gradients. This has profound implications for conservation, suggesting that maintaining natural movement patterns and landscape connectivity is crucial for fostering disease resilience and population heterogeneity.

11. Discussion

11.1. Advantages and limitations of the applied theoretical framework

The mathematical approaches employed in this study—ranging from stability analysis and Lyapunov functions to bifurcation theory and reaction–diffusion modeling—offer powerful tools for understanding complex eco–epidemiological dynamics. However, like any theoretical framework, they come with inherent advantages and limitations that warrant discussion.

11.1.1. Advantages

(1) **Comprehensive dynamical insights:** The combination of local stability analysis, global stability via Lyapunov functions, and bifurcation theory provides a multi–layered understanding of system behavior. This integrated approach reveals not only equilibrium states but also transient dynamics,

oscillatory behavior, and regime shifts—phenomena that are ecologically critical but often missed by simpler analyses.

(2) **Threshold parameter framework:** The derivation of five interconnected threshold parameters (R_0, R_0^*, R_1, $\bar{R}_1$, $\tilde{R}_1$) creates a unified language for discussing ecological and epidemiological invasion conditions. This framework translates complex mathematical conditions into biologically meaningful quantities that can, in principle, be estimated from field data.

(3) **Predictive power for regime shifts:** Bifurcation analysis, particularly the codimension–2 analysis identifying BT and CP points, provides early warning signals for critical transitions. This allows researchers to identify parameter regions where ecosystems may be vulnerable to sudden, irreversible changes—information vital for conservation planning.

(4) **Spatial realism:** The extension to reaction–diffusion systems incorporates the fundamental ecological reality that organisms move and interact across space. Turing pattern analysis demonstrates how purely local interactions can generate large–scale spatial heterogeneity, explaining phenomena like disease refuges and traveling epidemic waves without invoking environmental gradients.

(5) **Rigorous mathematical foundation:** The use of Lyapunov functions (Theorem 5.5) provides global stability results that are stronger than local linearizations, ensuring that conclusions about system behavior are not merely artifacts of initial condition choices.

11.1.2. Limitations and caveats

(1) **Model simplifications:** The model, even though comprehensive, must simplify biological reality. Key assumptions include:

- No recovery or immunity from infection (assumption A6).
- No horizontal transmission among predators.
- Constant parameter values, ignoring environmental stochasticity.
- Well–mixed populations in the non–spatial model.

These simplifications, while mathematically tractable, may limit their direct applicability to specific real–world systems where these factors are significant.

(2) **Analytical intractability of the full system:** Due to the four–dimensional nature of the system and the nonlinearities in the functional responses, a complete analytical characterization of the interior equilibrium $\tilde{\mathbf{E}}$ proved infeasible. The stability analysis of this ecologically significant state relies heavily on numerical continuation methods (e.g., MatCont), which, while powerful, explore only a finite region of parameter space and may miss behaviors in unexamined regions.

(3) **Lyapunov function construction:** While we successfully constructed Lyapunov functions for specific cases (Theorem 5.5), there is no systematic method for constructing such functions for general four–dimensional nonlinear systems. The functions presented are tailored to specific equilibria and may not exist or be discoverable for all parameter regimes.

(4) **Numerical limitations:** Numerical bifurcation analysis, while essential, has inherent limitations:

- Results depend on numerical continuation algorithms and step–size choices.
- Detection of homoclinic and heteroclinic bifurcations near codimension–2 points requires high numerical precision.

- The high–dimensional phase space makes comprehensive exploration computationally expensive.

(5) **Parameter estimation challenges:** The model contains numerous parameters (r, K, λ_1, λ_2, α_1, α_2, a_1, a_2, β, γ_1, γ_2, and μ) and diffusion coefficients (D_i). Estimating these simultaneously from empirical data presents formidable challenges, potentially limiting the model's practical application in data–poor scenarios.

(6) **Spatial model simplifications:** The reaction–diffusion framework, while incorporating space, assumes homogeneous diffusion coefficients and simple zero–flux boundary conditions. Real ecosystems exhibit heterogeneous movement patterns, anisotropic dispersal, and complex boundary interactions that this framework cannot capture. Additionally, the Turing instability analysis assumes small perturbations around homogeneous steady states, potentially missing pattern formation mechanisms far from equilibrium.

(7) **Cross–scale integration:** The model operates at the population level but makes implicit assumptions about individual behavior (e.g., mass–action incidence and Holling type II functional response). Bridging these scales remains an ongoing challenge in theoretical ecology, and individual–level variations that could significantly impact outcomes (e.g., heterogeneous susceptibility and behavioral adaptations) are not captured.

11.1.3. Methodological trade–offs and future directions

The theoretical choices in this study reflect necessary trade–offs between mathematical tractability and biological realism. The Holling type II functional response, for instance, captures saturated predation more realistically than type I. However, it introduces additional nonlinearities that complicate our analysis. Similarly, the decision to exclude predator–predator transmission simplifies the mathematics but may underestimate disease persistence in systems where such transmission occurs.

Future work could address some limitations through:

- **Stochastic extensions:** Incorporating demographic and environmental stochasticity to assess deterministic predictions' robustness.
- **Individual–based models:** Validating mean–field predictions against agent–based simulations that relax mixing assumptions.
- **Data assimilation:** Developing Bayesian parameter estimation frameworks to connect the model with empirical time series.
- **Adaptive behavior:** Incorporating predator or prey behavioral responses to infection risk.
- **Seasonal forcing:** Exploring how periodic parameter variations interact with the bifurcation structure identified here.

Despite these limitations, the theoretical framework presented provides a rigorous foundation for understanding cross–species disease transmission in predator–prey systems. The thresholds, stability conditions, and bifurcation structures identified offer testable hypotheses and conceptual tools for interpreting observed eco–epidemiological patterns.

11.2. Sensitivity to parameter variations and the role of Allee effects

Understanding how parameter variations shape system dynamics is fundamental to both theoretical insights and practical management applications. Below, we discuss the ecological implications of

parameter sensitivity. We provide a detailed discussion of the Allee effect, its ecological significance, and why its explicit incorporation represents a valuable future extension of the current framework.

11.2.1. Ecological impact of parameter variations

The nine distinct dynamical regimes summarized in Table 1 demonstrate the profound sensitivity of the predator–prey–disease system to parameter variations. Each parameter carries a specific ecological meaning and its variation can trigger qualitatively different outcomes:

- **Carrying capacity (K):** Increasing K amplifies both $R_0 = K\lambda_1/\mu$ and $R_1 = \beta K/[\gamma_1(1 + a_1K)]$, simultaneously enhancing disease persistence potential and predator invasion success. The nonlinear relationship in R_1 (saturating due to the Holling–type functional response) means that beyond a certain K, further increases predominantly affect disease dynamics rather than predator persistence. This explains the transition from Case 2 ($R_0 > 1$, $R_1 < 1$) to Case 5 ($R_0 > R_0^* > 1$) as K increases—disease becomes sufficiently prevalent to exclude predators that would otherwise persist.
- **Disease transmission rate (λ_1):** This parameter directly controls the basic reproductive number R_0 and the coexistence disease number R_0^*. Low λ_1 (Cases 1–4) allows disease–free dynamics, while moderate values (Cases 5-6) create endemic prey states. High λ_1 (Case 7) can generate oscillatory disease dynamics. The threshold $\lambda_1 = \mu/K$ marks the invasion boundary–a critical management target for disease control.
- **Predator mortality (γ_1, γ_2):** These parameters inversely affect predator persistence. The codimension–2 analysis in the (γ_1, λ_1)–plane (Section 9) reveals that small increases in predator mortality can trigger catastrophic regime shifts when parameters lie near the BT point. This has direct conservation implications: Stressed predator populations (elevated γ_1) may suddenly collapse when disease pressure crosses critical thresholds.
- **Predation rates (α_1, α_2):** The inequality $\alpha_2 \geq \alpha_1$ (assumption A7) encodes the ecological reality that infected prey are more vulnerable. The magnitude of this difference determines whether predation acts as disease control (α_2 sufficiently high, Cases 6-7) or as a mechanism for disease–mediated predator extinction (α_2 only slightly exceeds α_1, Case 5). This parameter thus governs whether predators function as ecosystem doctors (removing diseased individuals) or become victims of the pathogens themselves.
- **Handling times (a_1, a_2):** These saturating parameters in the Holling type II functional responses determine how quickly predation efficiency declines with prey density. Small a_i (short handling times) maintain high predation rates even at high prey densities, stabilizing dynamics. Large a_i (long handling times) introduce nonlinearities that can generate oscillatory behavior and Hopf bifurcations when R_1 exceeds $1 + \beta/[a_1\gamma_1(1 + a_1K)]$.

The practical benefit of understanding these parameter sensitivities lies in targeted management: Interventions can focus on parameters to which the system is most sensitive, maximizing conservation impact with limited resources. For instance, if a system operates near the BT point, even small reductions in predator mortality (γ_1) or disease transmission (λ_1) could avert catastrophic collapse.

11.2.2. The Allee effect: ecological significance and model implications

The Allee effect, named after ecologist Walter Allee, describes a positive relationship between population density and per–capita growth rate at low population sizes [27]. In contrast to the logistic growth assumption used in our model (where per–capita growth rate is maximized at low densities), the Allee effect creates extinction thresholds below which populations inevitably decline to zero. This phenomenon has profound implications for predator–prey disease systems and represents a natural extension of current work.

Ecological mechanisms of Allee effects: Allee effects arise from multiple mechanisms relevant to our system:

- **Mate finding limitation:** At low prey densities, individuals struggle to locate mates, reducing reproduction.
- **Predator dilution:** At low prey densities, each individual faces higher predation risk.
- **Cooperative defense:** Many prey species depend on group vigilance or mobbing for predator deterrence.
- **Foraging efficiency:** Some predators hunt more effectively in groups (pack hunting).
- **Environmental conditioning:** Population density may affect habitat quality.

Mathematical formulations: The logistic growth term $rS(1–(S + I)/K)$ in our model could be modified to incorporate Allee effects in several ways:

(1) **Multiplicative Allee effect:**

$$rS\left(1–\frac{S + I}{K}\right)\left(\frac{S + I}{A}–1\right),$$

where A is the Allee threshold. Populations below A experience negative growth.

(2) **Additive Allee effect:**

$$rS\left(1–\frac{S + I}{K}\right)–\frac{m}{1 + (S + I)},$$

representing increased mortality at low densities.

(3) **Component Allee effect:**
Modifying predation terms to reflect reduced group defense at low densities.

Predicted dynamical consequences: Incorporating Allee effects would fundamentally alter our system's dynamics in ways that extend beyond the current findings:

(1) **Extinction thresholds:** The trivial equilibrium $E_0 = (0, 0, 0, 0)$ could become locally stable, creating a true extinction basin. This adds a third attractor to the bistable scenarios (Case 8), potentially generating stability among extinction, disease–free coexistence, and endemic states.

(2) **Enhanced bistability:** Allee effects typically enlarge the parameter regions where multiple stable states coexist. The CP bifurcation identified in our codimension–2 analysis would likely split into two separate saddle–node bifurcations, creating a hysteresis loop with three equilibrium branches—a phenomenon known as a double saddle–node or S–shaped bifurcation diagram.

(3) **Critical slowing down:** Near extinction thresholds, systems exhibit critical slowing down—recovery from perturbations becomes slower. This provides early warning signals detectable in time series data, offering practical management tools.
(4) **Disease–mediated Allee effects:** The interaction between Allee effects and disease creates novel feedbacks. Infected prey, already vulnerable, may further reduce prey densities below Allee thresholds, accelerating extinction. Conversely, selective predation on infected prey might push the pathogen to extinction while leaving prey above their Allee threshold—a potential conservation strategy.
(5) **Spatial implications:** In the reaction–diffusion framework, Allee effects interact with diffusion to create propagating fronts with minimum patch size requirements for persistence. This could refine the Turing pattern analysis: Spots might need to exceed critical sizes to function as disease refuges, and striped epidemic waves might fail to propagate through low–density regions.

Management implications: The presence of Allee effects fundamentally changes conservation strategies:

- **Minimum viable populations:** Management must maintain populations above Allee thresholds, not just positive growth rates.
- **Translocation success:** Reintroduction programs must release sufficient individuals to exceed Allee thresholds.
- **Disease control:** Culling strategies that reduce prey below the Allee threshold risk catastrophic collapse, even if disease control is achieved.
- **Habitat fragmentation:** Spatial subdivision may create subpopulations below Allee thresholds, increasing extinction risk.

Why Allee effects were not included in this study: The decision to exclude Allee effects from the current model reflects a deliberate trade–off between biological complexity and mathematical tractability. Our four–dimensional system already exhibits extraordinary dynamical richness, including multiple codimension–2 bifurcations and Turing patterns. Added Allee effects would:

(1) Increase the system dimension or introduce additional nonlinearities, potentially precluding analytical progress.
(2) Compound the analytical complexity of the interior equilibrium, which already resists full characterization.
(3) Introduce additional parameters (A, m) that would require estimation and complicate interpretation.
(4) Risk obscuring the fundamental mechanisms of cross–species transmission that are the paper's central focus.

Future research directions: The detailed discussion above serves as a roadmap for future investigations. Natural extensions of this work include:

(1) Incorporating a strong Allee effect in prey growth and analyzing its impact on the five threshold parameters.

(2) Investigating how Allee thresholds interact with R_0 and R_1 to create extinction vortices.
(3) Extending the spatial analysis to examine how diffusion interacts with Allee effects to determine minimum patch sizes for persistence.
(4) Developing management frameworks that simultaneously account for disease transmission and Allee thresholds.

In conclusion, while our current model focuses on the novel mechanism of cross–species transmission, parameter sensitivity analysis reveals the system's rich behavioral repertoire. The Allee effect, though not explicitly modeled, represents a biologically significant phenomenon. Its incorporation would likely amplify the multi–mutability and critical transition phenomena already documented, while introducing more protective extinction thresholds of direct conservation relevance.

11.3. Ecological regimes and real–world analogues

The six dynamical regimes identified in the (γ_1, λ_1)–parameter plane (Table 2, Figure 11) correspond to distinct ecological scenarios observable in nature:

- **Region I (Low γ_1, Low λ_1): Stable disease–free coexistence** *Ecological analogue:* Healthy predator–prey systems with low disease prevalence, such as well–managed national parks where wildlife populations coexist stably with minimal disease impact. Predators effectively regulate prey without causing cycles, and diseases fail to establish due to low transmission rates.
  Example: Wolf–elk systems in Yellowstone prior to chronic wasting disease emergence.
- **Region II (Moderate γ_1, Low λ_1): Stable endemic coexistence** *Ecological analogue:* Systems where diseases persist at low, stable levels within prey populations, and predators have adapted to coexist with infected prey. The disease becomes part of the ecosystem's background, neither exploding into epidemics nor driving host extinction.
  Example: Bovine tuberculosis in African buffalo populations with lion predation.
- **Region III (High γ_1, Any λ_1): Predator extinction** *Ecological analogue:* Systems where predator mortality exceeds replacement capacity, leading to predator loss. This can result from direct persecution (hunting), habitat loss, or disease–induced mortality. Without predators, prey populations may be regulated primarily by disease or carrying capacity.
  Example: Fragmented forest patches where large predators have been extirpated, leaving prey populations susceptible to disease outbreaks.
- **Region IV (Moderate γ_1, High λ_1): Oscillatory coexistence** *Ecological analogue:* Classic predator–prey cycles modified by disease dynamics. Populations exhibit regular fluctuations, often with characteristic periods. Disease prevalence may peak following prey peaks, creating complex multi–year cycles.
  Example: Feline immunodeficiency virus (FIV) in African lion populations, where disease prevalence fluctuates with prey abundance cycles.
- **Region V (Near CP Point): Bistability and historical contingency** *Ecological analogue:* Systems where two alternative stable states exist–either disease–free coexistence or endemic prey–only. Which state occurs depends on historical accidents: a pathogen introduction event, a drought, or human intervention can flip the system between states. Restoration may require crossing thresholds in the opposite direction (hysteresis).

Example: Tasmanian devil facial tumor disease, where populations can persist at reduced densities with endemic disease or, under different conditions, face local extinction. The system exhibits bistability depending on devil density and disease transmission rates.

- **Region VI (Near BT Point): Complex transients and critical transitions** *Ecological analogue:* Systems poised near ecological tipping points, where small perturbations can trigger dramatic, hard–to–predict transitions. Population dynamics exhibit complex transient behaviors, including "canard cycles"—trajectories that alternate between small–amplitude oscillations near equilibrium and large–amplitude excursions.
  Example: Arctic ecosystems experiencing rapid climate change, where predator–prey dynamics (e.g., arctic fox–lemming cycles) become highly unpredictable near critical temperature thresholds, potentially leading to sudden regime shifts.

11.4. Conservation and disease management implications

Our results yield concrete, actionable insights for wildlife management.

(1) **Predator conservation as disease control:** Cases 6-7 demonstrate that selective predation can eradicate disease from prey populations. This suggests that maintaining healthy predator populations may serve as a cost–effective, natural disease control strategy. For example, in ecosystems affected by CWD in deer, maintaining wolf or cougar populations that selectively prey on infected individuals could help suppress disease spread—a hypothesis supported by our model when α_2 (predation on infected prey) is sufficiently high.

(2) **Risks of predator culling:** The model warns that culling predators–a common management response to perceived over–predation or human–wildlife conflict—may inadvertently increase disease prevalence. When $R_0^* < 1 < R_0$ (Cases 6-7), predators are actively suppressing disease. Removing them could trigger disease outbreaks with greater economic and conservation impacts than the original predation concern. This has direct relevance to debates over wolf culling in North America and Europe.

(3) **Threshold–based monitoring:** The five threshold parameters provide a monitoring framework for wildlife managers:

- Monitor R_0 to predict disease outbreaks in prey populations.
- Monitor R_1 to assess predator population viability.
- Monitor R_0^* to evaluate whether predator–prey communities can resist disease invasion.
- Track $\overline{R}_1$ and $\widetilde{R}_1$ to assess how endemic disease affects predator persistence.

These thresholds can be estimated from field data on reproduction, mortality, and transmission rates, providing early warning of critical transitions.

(4) **CP–induced hysteresis and restoration challenges:** The bistability near the CP point (Region V) implies that restoring degraded ecosystems may require pushing parameters beyond original tipping points. For example, if disease has driven a system to an endemic prey–only state (loss of predators), simply reducing disease transmission to pre–outbreak levels may not restore predators. Active reintroduction and temporary predator support may be necessary to cross the hysteresis loop. This has direct implications for rewilding projects and species reintroduction programs.

(5) **Spatial patterns and reserve design:** The Turing patterns identified in Section 10 have profound implications for conservation planning:

- **Spot patterns (disease refuges):** When predator diffusion dominates ($D_{P_1}, D_{P_2} \gg D_S, D_I$), isolated prey clusters emerge that can persist disease–free. Reserve designs should maintain connectivity between such refuges while allowing predator movement that creates this pattern.
- **Striped patterns (epidemic waves):** When diffusion rates are similar, traveling waves of infection emerge. This suggests that linear habitat features (rivers, ridges, and corridors) may channel disease spread, and management interventions (vaccination corridors, culling barriers) should be oriented perpendicular to predicted wave fronts.
- **Minimum patch size requirements:** The Allee effect discussion (Section 11.2.2) suggests that disease refuges must exceed critical sizes to persist. This provides quantitative targets for protected area design: Fragments below threshold size may lose their refuge function even if habitat quality is maintained.

11.5. Testable ecological predictions

Our model generates several empirically testable predictions that could guide future field studies.

(1) **Predator density–disease prevalence relationship:** The model predicts a non–monotonic relationship between predator density and disease prevalence in prey. At low predator densities ($R_1 < 1$), predators are absent, and disease dynamics follow R_0. At moderate predator densities ($1 < R_1 < 1 + \frac{\beta}{a_1\gamma_1(1+a_1K)}$), selective predation suppresses disease ($R_0^* < 1$). At high predator densities, oscillatory dynamics emerge with fluctuating disease prevalence. Field studies comparing disease prevalence across gradients of predator density could test this prediction.

(2) **Disease–mediated predator extinction threshold:** The condition $R_0 > R_0^* > 1$ identifies when disease drives predator extinction despite predators being viable in disease–free conditions ($R_1 > 1$). This predicts that pathogen introduction into predator–prey systems can trigger predator collapse even without direct predator infection—a phenomenon observable in systems where novel pathogens emerge in prey populations.

(3) **Alternative stable states in disease management:** The bistability region (Case 8) predicts that identical environmental conditions can support qualitatively different community states. This suggests that intervention history matters: Two seemingly identical ecosystems may differ in disease status due to past culling, reintroduction, or disease introduction events. Long–term monitoring across multiple sites could reveal such historical contingency.

(4) **Spatial pattern–diffusion relationship:** The Turing analysis predicts that the ratio of predator to prey diffusion coefficients determines spatial pattern type (spots vs. stripes). This could be tested in controlled mesocosm experiments with manipulated dispersal rates or in natural systems where movement rates vary across habitat types.

(5) **Allee threshold–disease interaction:** The theoretical discussion of Allee effects predicts that disease introduction near Allee thresholds can trigger rapid extinction—a phenomenon observable in small, isolated populations of conservation concern. This suggests that disease surveillance should be prioritized in populations already near minimum viable population sizes.

12. Conclusions

This study provides a comprehensive analysis of a predator–prey model with cross–species disease transmission, highlighting the profound interplay between ecological and epidemiological processes. The key outcomes are:

(1) **Unified threshold framework**: We derive five interconnected threshold parameters (R_0, R_0^*, R_1, $\overline{R}_1$, and $\widetilde{R}_1$) that govern disease invasion and predator persistence. The hierarchy $\overline{R}_1 < \widetilde{R}_1 < R_1$ quantitatively shows how disease presence progressively challenges predator persistence, creating a disease–mediated predation pressure.
(2) **Global stability**: Using a novel Lyapunov function, we prove that under specific conditions ($R_0^* < 1$ and a stable disease–free subsystem), the system converges globally to a healthy predator–prey state. This provides a theoretical basis for predators to act as self–sustaining biological control agents.
(3) **Organizing centers**: Bifurcation analysis reveals codimension–2 points (BT and CP) that act as ecological epicenters. These points organize the system's dynamics, explaining extreme parameter sensitivity, the emergence of canard cycles, and the presence of tipping points and hysteresis between alternative stable states.
(4) **Dual roles**: The model uncovers opposing but significant roles: Disease can act as a super–predator, driving predators to extinction (Case 5); conversely, selective predation on infected prey can eradicate disease, providing a crucial ecosystem service (Cases 6-7).
(5) **Bistability**: The existence of alternative stable states (Case 8) demonstrates that historical contingency can determine ecosystem fate. This warns that restoring environmental conditions may not guarantee recovery if the system has crossed a threshold into a degraded state with hysteresis.
(6) **Spatial self–organization**: The reaction–diffusion extension shows that predator–prey–disease systems can spontaneously form turing patterns. Spot patterns create natural disease refuges, while striped patterns represent epidemic waves, offering vital insights into conservation planning and reserve design.
(7) **Comprehensive bifurcation map**: The two–parameter bifurcation diagram serves as an ecological map, identifying six distinct dynamical regimes and danger zones of high sensitivity. This provides a practical tool for anticipating ecosystem responses to environmental changes and guiding management interventions.

In conclusion, this work demonstrates that predator–prey–disease systems are not mere extensions of their components but exhibit qualitatively distinct behaviors like bistability, canard cycles, and spatial patterns. The integrated analytical and numerical framework presented here advances the mathematical theory of eco–epidemiology and provides practical insights into biodiversity conservation and disease control in an era of rapid environmental change.

Author contributions

The authors confirm their contribution to the paper as follows: study conception and design: Faisal Muteb K. Almalki, Ghaliah Alhamzi, Sayed Saber; model formulation and analysis: Ghaliah Alhamzi,

Emad Solouma, Sayed Saber; numerical simulations and bifurcation analysis: Emad Solouma, Sayed Saber, Mona Bin–Asfour; spatial extension analysis: Najat Almutairi, Ali Sarrah, Faisal Muteb K. Almalki; drafting of the manuscript: all authors; critical revision and final approval: all authors. All authors have read and agreed to the published version of the manuscript.

Use of Generative–AI tools declaration

The authors declare that no generative artificial intelligence (AI) tools were used in the writing, analysis, or preparation of this manuscript. All mathematical derivations, numerical simulations, and analyses were performed by the authors using standard computational tools (MATLAB, MatCont) without the assistance of AI–based text or code generation.

Funding

This work was supported and funded by the Deanship of Scientific Research at Imam Mohammad Ibn Saud Islamic University (IMSIU) (grant number IMSIU–DDRSP2601).

Conflict of interest

The author declares that they have no conflicts of interest.

References

1. R. M. May, *Stability and complexity in model ecosystems*, Princeton University Press, 1974.
2. C. S. Holling, The components of predation as revealed by a study of small-mammal predation of the European pine sawfly, *Can. Entomol.*, **91** (1959), 293–320. https://doi.org/10.4039/Ent91293-5
3. P. H. Leslie, Some further notes on the use of matrices in population mathematics, *Biometrika*, **35** (1948), 213–245. https://doi.org/10.2307/2332342
4. A. Korobeinikov, A Lyapunov function for Leslie-Gower predator-prey models, *Appl. Math. Lett.*, **14** (2001), 697–700. https://doi.org/10.1016/S0893-9659(01)80029-X
5. H. W. Hethcote, W. Wang, L. Han, Z. Ma, A predator-prey model with infected prey, *Theor. Popul. Biol.*, **66** (2004), 259–268. https://doi.org/10.1016/j.tpb.2004.06.010
6. X. Chen, W. Yang, Complex dynamical behaviors of a Leslie-Gower predator-prey model with herd behavior, *J. Nonlinear Model. Anal.*, **6** (2024), 1064–1082. https://doi.org/10.12150/jnma.2024.1064
7. Y. Li, M. He, Z. Li, Dynamics of a ratio-dependent Leslie-Gower predator-prey model with Allee effect and fear effect, *Math. Comput. Simul.*, **201** (2022), 417–439. https://doi.org/10.1016/j.matcom.2022.05.017
8. W. Ding, W. Huang, Global dynamics of a ratio-dependent Holling-Tanner predator-prey system, *J. Math. Anal. Appl.*, **460** (2018), 458–475. https://doi.org/10.1016/j.jmaa.2017.11.057

9. Y. Liu, Z. Zhang, Z. Li, The impact of Allee effect on a Leslie-Gower predator-prey model with hunting cooperation, *Qual. Theory Dyn. Syst.*, **23** (2024), 88. https://doi.org/10.1007/s12346-023-00940-7
10. W. Yin, Z. Li, F. Chen, M. He, Modeling Allee effect in the Leslie-Gower predator-prey system incorporating a prey refuge, *Int. J. Bifurcation Chaos*, **32** (2022), 2250086. https://doi.org/10.1142/S0218127422500869
11. C. Arancibia-Ibarra, J. D. Flores, G. Pettet, P. van Heijster, A Holling-Tanner predator-prey model with strong Allee effect, *Int. J. Bifurcation Chaos*, **29** (2019), 1930032. https://doi.org/10.1142/s0218127419300325
12. Y. Dai, Y. Zhao, B. Sang, Four limit cycles in a predator-prey system of Leslie type with generalized Holling type III functional response, *Nonlinear Anal. Real World Appl.*, **50** (2019), 218–239. https://doi.org/10.1016/j.nonrwa.2019.04.003
13. J. Ren, X. Li, Bifurcations in a seasonally forced predator-prey model with generalized Holling type IV functional response, *Int. J. Bifurcation Chaos*, **26** (2016), 1650203. https://doi.org/10.1142/S0218127416502035
14. J. B. Collings, The effects of the functional response on the bifurcation behavior of a mite predator-prey interaction model, *J. Math. Biol.*, **36** (1997), 149–168. https://doi.org/10.1007/s002850050095
15. M. Zhang, Z. Li, F. Chen, L. Chen, Bifurcation analysis of a Leslie-Gower predator-prey model with Allee effect on predator and simplified Holling type IV functional response, *Qual. Theory Dyn. Syst.*, **24** (2025), 131. https://doi.org/10.1007/s12346-025-01291-1
16. C. Huangfu, Z. Li, F. Chen, L. Chen, M. He, Dynamics of a harvested Leslie-Gower predator-prey model with simplified Holling type IV functional response, *Int. J. Bifurcation Chaos*, **25** (2025), 550023. https://doi.org/10.1142/S0218127425500233
17. D. Xiao, S. Ruan, Codimension two bifurcations in a predator-prey system with group defense, *Int. J. Bifurcation Chaos*, **11** (2001), 2123–2131. https://doi.org/10.1142/S021812740100336X
18. M. A. Aziz-Alaoui, M. Daher Okiye, Boundedness and global stability for a predator-prey model with modified Leslie-Gower and Holling-type II schemes, *Appl. Math. Lett.*, **16** (2003), 1069–1075. https://doi.org/10.1016/S0893-9659(03)90096-6
19. A. F. Nindjin, M. A. Aziz-Alaoui, M. Cadivel, Analysis of a predator-prey model with modified Leslie-Gower and Holling-type II schemes with time delay, *Nonlinear Anal. Real World Appl.*, **7** (2006), 1104–1118. https://doi.org/10.1016/j.nonrwa.2005.10.003
20. H. Wu, Z. Li, M. He, Bifurcation analysis of a Holling-Tanner model with generalist predator and constant-yield harvesting, *Int. J. Bifurcation Chaos*, **34** (2024), 2450076. https://doi.org/10.1142/S0218127424500767
21. D. Xiao, S. Ruan, Global analysis in a predator-prey system with nonmonotonic functional response, *SIAM J. Appl. Math.*, **61** (2001), 1445–1472. https://doi.org/10.1137/S0036139999361896

22. M. Yuan, N. Wang, Stability and bifurcation analysis for a predator-prey model with Crowley-Martin functional response, *J. Nonlinear Model. Anal.*, **7** (2025), 1–19. https://doi.org/10.12150/jnma.2025.1

23. Y. Yang, Y. Xu, L. Rong, S. Ruan, Bifurcations and global dynamics of a predator-prey mite model of Leslie type, *Stud. Appl. Math.*, **152** (2024), 1251–1304. https://doi.org/10.1111/sapm.12675

24. M. He, Z. Li, Global dynamics of a Leslie-Gower predator-prey model with square root response function, *Appl. Math. Lett.*, **140** (2023), 108561. https://doi.org/10.1016/j.aml.2022.108561

25. S. Hsu, T. Huang, Global stability for a class of predator-prey systems, *SIAM J. Appl. Math.*, **55** (1995), 763–783. https://doi.org/10.1137/S0036139993253201

26. E. Sáez, E. González-Olivares, Dynamics of a predator-prey model, *SIAM J. Appl. Math.*, **59** (1999), 1867–1878. https://doi.org/10.1137/S0036139997318457

27. D. Sen, S. Ghorai, S. Sharma, M. Banerjee, Allee effect in prey's growth reduces the dynamical complexity in prey-predator model with generalist predator, *Appl. Math. Model.*, **91** (2021), 768–790. https://doi.org/10.1016/j.apm.2020.09.046

28. Y. Zhang, J. Huang, H. Wang, Bifurcations driven by generalist and specialist predation: mathematical interpretation of Fennoscandia phenomenon, *J. Math. Biol.*, **86** (2023), 94. https://doi.org/10.1007/s00285-023-01929-1

29. C. Xiang, J. Huang, S. Ruan, D. Xiao, Bifurcation analysis in a host-generalist parasitoid model with Holling II functional response, *J. Differ. Equations*, **268** (2020), 4618–4662. https://doi.org/10.1016/j.jde.2019.10.036

30. S. Dey, S. Ghorai, M. Banerjee, Analytical detection of stationary and dynamic patterns in a prey-predator model with reproductive Allee effect in prey growth, *J. Math. Biol.*, **87** (2023), 21. https://doi.org/10.1007/s00285-023-01957-x

31. S. Li, S. Yuan, Z. Jin, H. Wang, Bifurcation analysis in a diffusive predator-prey model with spatial memory of prey, Allee effect and maturation delay of predator, *J. Differ. Equations*, **357** (2023), 32–63. https://doi.org/10.1016/j.jde.2023.02.009

32. X. Li, J. Ren, S. A. Campbell, G. S. K. Wolkowicz, H. Zhu, How seasonal forcing influences the complexity of a predator-prey system, *Discrete Contin. Dyn. Syst. Ser. B*, **23** (2018). https://doi.org/10.3934/dcdsb.2018043

33. R. A. Taylor, J. A. Sherratt, A. White, Seasonal forcing and multi-year cycles in interacting populations: lessons from a predator-prey model, *J. Math. Biol.*, **67** (2013), 1741–1764. https://doi.org/10.1007/s00285-012-0612-z

34. S. Rinaldi, S. Muratori, Y. Kuznetsov, Multiple attractors, catastrophes and chaos in seasonally perturbed predator-prey communities, *Bull. Math. Biol.*, **55** (1993), 15–35.

35. J. M. Tuwankotta, E. Harjanto, Strange attractors in a predator-prey system with non-monotonic response function and periodic perturbation, *J. Comput. Dyn.*, **6** (2019), 469–483. https://doi.org/10.3934/jcd.2019024

36. Y. A. Kuznetsov, S. Muratori, S. Rinaldi, Bifurcations and chaos in a periodic predator-prey model, *Int. J. Bifurcation Chaos*, **2** (1992), 117–128. https://doi.org/10.1142/S0218127492000112

37. M. Alhazmi, S. Saber, Glucose-insulin regulatory system: Chaos control and stability analysis via Atangana–Baleanu fractal-fractional derivatives, *Alex. Eng. J.*, **122** (2025), 77-90. https://doi.org/10.1016/j.aej.2025.02.066

38. S. Saber, E. Solouma, Advanced fractional modeling of diabetes: bifurcation analysis, chaos control, and a comparative study of numerical methods Adams–Bashforth–Moulton and Laplace–Adomian–Padé method, *Indian J. Phys.*, **99** (2025), 5151–5169. https://doi.org/10.1007/s12648-025-03712-y

39. S. Saber, S. M. Mirgani, Numerical solutions, stability, and chaos control of Atangana–Baleanu variable-order derivatives in glucose-insulin dynamics, *J. Appl. Math. Comput. Mech.*, **24** (2025), 44–55. https://doi.org/10.17512/jamcm.2025.1.04

40. A. Alsulami, R. A. Alharb, T. M. Albogami, N. H. E. Eljaneid, H. D. S. Adam, S. F. Saber, Controlled chaos of a fractal–fractional Newton-Leipnik system, *Therm. Sci.*, **28** (2024), 5153–5160. https://doi.org/10.2298/TSCI2406153A

41. T. Yan, M. Alhazmi, M. Y. Youssif, A. E. Elhag, A. F. Aljohani, S. Saber, Analysis of a Lorenz model using adomian decomposition and fractal-fractional operators, *Therm. Sci.*, **28** (2024), 5001–5009. https://doi.org/10.2298/TSCI2406001Y

42. M. Alhazmi, F. M. Dawalbait, A. Aljohani, K. O. Taha, H. D. S. Adam, S. Saber, Numerical approximation method and chaos for a chaotic system in sense of Caputo-Fabrizio operator, *Therm. Sci.*, **28** (2024), 5161–5168. https://doi.org/10.2298/TSCI2406161A

43. P. A. Naik, R. Ahmed, S. Q. Shahzad, Z. Huang, Exploring dynamic behavior in a two-dimensional discretized predator-prey model using piecewise constant argument method, *Int. J. Dyn. Control*, **13** (2025), 389. https://doi.org/10.1007/s40435-025-01916-y

44. M. M. Khan, M. J. Uddin, P. A. Naik, Z. Eskandari, Z. Huang, Bifurcation analysis, chaos control and complex dynamics of a discrete prey-predator system incorporating an Ivlev functional response with an Allee effect, *Qual. Theory Dyn. Syst.*, **24** (2025), 169. https://doi.org/10.1007/s12346-025-01332-9

45. P. A. Naik, M. Amer, R. Ahmed, S. Qureshi, Z. Huang, Stability and bifurcation analysis of a discrete predator-prey system of Ricker type with refuge effect, *Math. Biosci. Eng.*, **21** (2024), 4554–4586. https://doi.org/10.3934/mbe.2024201

46. P. A. Naik, R. Ahmed, A. Faizan, Theoretical and numerical bifurcation analysis of a discrete predator-prey system of Ricker type with weak Allee effect, *Qual. Theory Dyn. Syst.*, **23** (2024), 260. https://doi.org/10.1007/s12346-024-01124-7

47. M. J. Uddin, P. A. Naik, Z. Eskandari, S. Monira, Z. Huang, Complex dynamics and chaos control in a fractional-order discrete prey-predator model incorporating an Ivlev functional response and Allee effect, *Math. Comput. Simul.*, **241** (2026), 300–325. https://doi.org/10.1016/j.matcom.2025.08.024

48. S. Saber, E. Solouma, R. A. Alharb, A. Alalyani, Chaos in fractional-order glucose–insulin models with variable derivatives: insights from the Laplace–Adomian decomposition method and generalized Euler techniques, *Fractal Fract.*, **9** (2025), 149. https://doi.org/10.3390/fractalfract9030149

49. S. Saber, S. M. Mirgani, Numerical analysis and stability of a system using the Laplace residual power series method incorporating the Atangana–Baleanu derivative, *Int. J. Model. Simul. Sci. Comput.*, **16** (2025), 2550030. https://doi.org/10.1142/S1793962325500308

50. S. Saber, S. M. Mirgani, Analyzing fractional glucose-insulin dynamics using Laplace residual power series methods via the Caputo operator: stability and chaotic behavior, *Beni-Suef Univ. J. Basic Appl. Sci.*, **14** (2025), 28. https://doi.org/10.1186/s43088-025-00608-y

51. A. Dhooge, W. Govaerts, Y. A. Kuznetsov, MATCONT: A MATLAB package for numerical bifurcation analysis of ODEs, *ACM Trans. Math. Softw.*, **29** (2003), 141–164. https://doi.org/10.1145/779359.779362

AIMS Press